OPTICAL MEASUREMENT OF DYE KINETICS AND ITS MEDICAL APPLICATION

Awazu, Kunio

(Degree)
博士（工学）
(Date of Degree)
1996-04-26
(Date of Publication)
2012-07-05
(Resource Type)
doctoral thesis
(Report Number)
乙2029
(JaLCDOI)
https://doi.org/10.11501/3117008
(URL)
https://hdl.handle.net/20.500.14094/D2002029

Doctoral Dissertation of Kobe University

OPTICAL MEASUREMENT OF DYE KINETICS

AND

ITS MEDICAL APPLICATION

March, 1996

Kunio Awazu

Doctoral Dissertation of Kobe University

OPTICAL MEASUREMENT OF DYE KINETICS

AND

ITS MEDICAL APPLICATION

（色素代謝の光学的計測とその医療応用）

March, 1996

Kunio Awazu

Abstract

In this thesis, the modeling of compartment system that can deal with the kinetics of the dyes is proposed, and lasers or light emission diodes as light sources are used for measuring fluorescence or transmittance of the target dyes. Using these methods, the compartmental analysis with experimental results of the fluorescence and the transmittance taken from collagen-membrane, rat-cancer-cells, or human-tissues gives the kinetics of the dyes. These results are studied with the viability of the rat-cancer-cells or human-liver-function. For the tissues considered optically scattering, mathematical simulation methods are proposed to evaluate the dependence of the scattering for the disappearance rates of the dye.

First of all, the fixation of a photosensitive reagent, tetrabrominated rhodamine (TBR), onto collagen gels is studied as a model for photolabeling biological tissues with medical reagents. Irradiation with a laser causes photo-induced debromination and subsequent covalent linkage of TBR to collagen. The study addresses the quantum efficiency of photolabeling, and how dimethylsulfoxide (DMSO) might enhance the efficiency of photolabeling. Video fluorescence assayed washed gels to measure the unbleached TBR affixed to a gel.

Next, the variation in photodynamic dose achieved with protoporphyrin IX (PPIX) and laser radiation is assessed in a cancer cell culture. The metabolic precursor d-aminolevulenic acid is included in the incubation media for 24 hour to induce cellular accumulation of protoporphyrin IX (PPIX) for the purpose of photodynamic therapy (PDT). The distributions of initial PPIX concentration, photobleaching light dose, and photodynamic dose, are measured on 124 individual cells using video laser fluorescence microscopy. Using the survival of the cells and the photodynamic dose given, a PDT protocol is proposed.

The measurement methods for the dye disappearances are expanded to a non-invasive method to determine indocyanine green, ICG, dye clearance from the liver. The study of ICG clearance in blood is clinically used for the estimation of hepatic function especially in Japan. Multiple blood samplings, however, subject the patients to mental and physical stress. Furthermore, although it is necessary with this method to correctly measure the blood sampling time after ICG injection, it is difficult to accurately measure this time in an actual test.. Thus, a measuring method without blood sampling has been desired. In this chapter, a description of an instrument for the non-invasive measurement of ICG clearance using an optical sensor attached to the fingertip is presented, and a calibration method before ICG injection is proposed to solve the problem of changing blood volume. Next, the results of the clinical evaluation are presented.

Finally, Monte Carlo simulation method and diffusion approximation method are proposed to examine the disappearance rate constants of ICG, the so called plasma disappearance rate from the liver. It is shown that the transmittance calculated by the diffusion theory is more stable than that by the Monte Carlo method to the slab model. The disappearance rates are estimated using an optically homogeneous turbid slab as a tissue model.

Contents

Abstract

CHAPTER 1 1
INTRODUCTION 1

1.1 Introduction and historical remarks 1
1.2 Outline of the thesis 4

CHAPTER 2 8
PHOTOLABELING OF A DYE TO MEASURE THE DISTRIBUTION OF LIGHT 8

2.1 Introduction 8
2.1.1 Compartmental model for TBR photoaffinity labeling and photobleaching 11
2.1.2 Quantum yields for photolabeling and photobleaching 17
2.2 Materials and methods 18
2.2.1 Chemicals 18
2.2.2 Collagen gel phantom 19
2.2.3 Laser exposure 20
2.2.4 Washing out unreacted TBR 23
2.2.5 Video fluorescence measurement 23
2.3 Results 24
2.3.1 Experiment 1: Kinetics of photolabeling and photobleaching 24
2.3.2 Experiment 2: Dependence of photolabeling on DMSO 30
2.4 Discussion 32
2.5 Conclusion 33

CHAPTER 3 34
PHOTOBLEACHING OF A DYE FOR CANCER CELLS 34

3.1 Introduction 34
3.1.1 Photobleaching and fluorescence 35
3.1.2 The photodynamic dose 36
3.2 Materials and methods 38
3.2.1 Cell cultures 38

3.2.2 Fluorescence assay for PPIX 39
3.2.3 Fluorescence microscopy 39
3.2.4 Cell digest fluorescence measurements (OMA) 42
3.2.5 Calibration experiments 43
3.2.5.1 Microscope calibration 43
3.2.5.2 OMA calibration 45
3.2.6 Colony formation 47
3.3 Results 48
3.3.1 Experimental data 48
3.3.2 Histograms 50
3.3.3 Bleb formation 54
3.3.4 Colony formation 56
3.4 Discussion 56
3.5 Conclusion 58

CHAPTER 4 59
METHOD FOR MEASURING DYE DILUTION IN BLOOD AND ITS CLINICAL EVALUATION 59

4.1 Introduction 59
4.1.1 Optical characteristics of ICG 60
4.1.2 ICG test using blood sampling 61
4.1.3 Prototype of continuous method 63
4.2 Materials and methods 65
4.2.1 The newly developed measuring algorithm 65
4.2.2 Optical sensor 67
4.2.3 The hardware system 69
4.3 Results 71
4.3.1 The system characteristics 71
4.3.2 Clinical evaluation 73
4.3.2.1 Method 73
4.3.2.2 Results 73
(1) Comparison with blood sampling method 73
(2) Values in hepatic diseases 76
4.6 Discussion 76
4.7 Conclusion 77

CHAPTER 5 79
NUMERICAL ANALYSES FOR ICG CLEARNACE
IN A TURBID MEDIA 79

5.1 Introduction 79
5.2 Materials and methods 81
5.2.1 Monte Carlo simulation 81
5.2.2 Diffusion theory 83
5.2.3 Optical model for the finger tip 88
5.3 Results 88
5.3.1 ICG optical property using a spectrophotometer 88
5.3.2 Simulation results of Monte Calro method
and diffusion approximation 90
5.3.3 Estimation of the decay constant of ICG using
the diffusion approximation 93
5.4 Discussion 99
5.5 Conclusion 99

CHAPTER 6 100
Conclusions 100

REFERENCES 103

ACKNOWLEDGMENTS 112

CHAPTER 1

INTRODUCTION

1.1 Introduction and historical remarks

In modern medical treatments, less invasively therapeutic or diagnostic systems are required. On the other hand, recent progress of electro optics (Hecht 1990), such as lasers (Siegman 1986, Verdeyen 1989), fiber-optics (Ezekiel 1982, Ohgoshi 1983), and semiconductor-devices (Steinmetz 1983) have contributed the fields of communication (Hahne 1987, Arnon 1994), information (Mollenauer 1980, Hasegawa 1981), measurement (Galliorenzi 1982, McMahon 1981) and so on. The main advantages on the usage of light are the minimum damage for the object, less electric magnetic interferance, and the ease of treating huge information (Yoshizawa 1985), so that the application of electro-optics to the medical treatments has been expected.

In the biomedical field, before the revolution in electro-optics, as an application of spectroscopy, testing hepatic function or measuring cardiac output using a dye such as indocyanine green (ICG) were investigated (Cherrick 1960, Leevy 1962) in the 1960s. In the 1970s, the optical fiber system in blood was modeled (Cheung 1973, Reynolds 1975), based on photon diffusion theory (Johnson

1970). Non-invasive skin and tissue reflectance oximeters were also developed (Takatani 1980) in the late 1970s. However, problems of the earlier workers included lack of adequate calibration procedure, unknown distribution of light in biological tissues, and lack of an appropriate mathematical relation to calculate the change of the dye concentration *in vivo*.

In the early 1980s, the noninvasive approach of pulse oximetry using opto-electronic devices, which combined the principle of conventional optical oximetry with the plethysmographic principle, offered a means of noninvasively estimation arterial blood oxygen saturation (Yelderman 1983, Pologe 1987). Most operation rooms and intensive care units today are equipped with this device (Kellerman 1991, Szaflarski 1989). This technique is based on the measuring the oxygen saturation of hemoglobin as a dye. Another innovative approach is the use of a very narrow light pulse to measure transmit time of light signals through tissue (Delpy 1988, Jacques 1991). This technique characterizes the tissue optical properties of absorption and scattering, from which absolute tissue oxygen saturation can be estimated (Chance 1988, Jacques, 1991). Furthermore, Photodynamic therapy (PDT) has been establishing as a new approach to cancer treatment in which photosensitizer localized in cancers are activated under visible light to interact with oxygen (Gomer 1989, Hampton 1992, Athar 1988, Wilson 1987, Henderson 1985).

These studies mentioned above are based on measuring dye's concentration using transmittance, reflectance or fluorescence of the dye in principle. In other words, each dye's specific absorption or fluorescence characteristic depending on wavelength is used to determine the relationship between the concentration or distribution of the dye in the biological tissues and diagnostic or therapeutic parameters. Particularly, the treatments appling dyes, such as PDT or ICG liver function tests using optical technique, are required adequate monochromatic lights such as lasers and detecting techniques to know the kinetics of the dye in cells or tissues for proposing less invasive protocols. Therefore, the kinetics of the dye *in vitro* or *in vivo* should be studied, in addition to measure the dye concentration, to know the radiation distribution in the target tissue, to estimate the effect of PDT for cells and to diagnose the hepatic function.

Developing optical methods that measure the fluorescence or optical properties of the target dye, and calibration methods that estimate the relationship between the measurement values and the dye concentration are required to know the kinetics of the dye. Furthermore, *in vivo* or *in vitro* evaluation is required to propose adequate protocols for treatments or diagnostic standards using the results of the kinetics.

1.2 Outline of this thesis

According to reasons mentioned above, the modeling of compartment systems that can deal with the kinetics of the dyes is proposed, and lasers or light emission diodes are used for measuring fluorescence or transmittance of the target dyes. Using these methods, the compartmental analysis with experimental results of the fluorescence and the transmittance taken from collagen-membrane, rat-cancer-cells, or human-fingertips give the kinetics of the dyes. This results are studied with the viability of the rat-cancer-cells or human-liver-function. For the tissues considered optically scattering, mathematical simulation methods are proposed to evaluate the dependence of the scattering for the disappearance rates of the dye.

In Chapter 2, knowing the radiation distribution in the tissue is discussed using the photo-chemical reaction. When a photon is absorbed by a molecular chromophore such as rhodamine and converts that molecule to an excited state, the laser energy has been converted into a stored form of chemical energy. The excited state may subsequently participate in a chemical reaction. The photon essentially behaves as a reagent that is consumed in the photochemical reaction as a photochemical product is produced. In a variety of such photochemical reactions, the fixation of a photosensitive reagent, tetrabrominated rhodamine (TBR), onto collagen gels is studied as a model for photolabeling biological tissues with medical reagents in this chapter. Irradiation with an Ar ion laser causes photo-induced debromination and subsequent covalent linkage of TBR to collagen. The study addresses(1) the quantum efficiency of photolabeling, and (2) how dimethylsulfoxide (DMSO) might enhance the efficiency of photolabeling. Video fluorescence assayed washed gels to measure the unbleached TBR affixed to a gel.

In Chapter 3, photodynamic therapy (PDT) for cells as a the microscopic application of the laser fluorescence measurement method described in Chapter 2 is discussed. PDT is a form of light -activated chemotherapy. A photosensitive dye such as porphirin is injected into the body, where it accumulates in certain cells, especially cancer cells. Irradiation with an appropriate-wavelength light source causes photon absorption by the dye, which yields an excited state. The excited state reacts with oxygen to generate toxic products such as singlet oxygen. These toxic products injure the local cellular environment, and the cells. In this chapter, the variation in photodynamic dose achieved with protoporphyrin IX (PPIX) and laser radiation is assessed in a cancer cell culture. The metabolic precursor δ–aminolevulenic acid is included in the incubation media for 24 hr to induce cellular accumulation of protoporphyrin IX (PPIX) for the purpose of photodynamic therapy (PDT). The distributions of initial PPIX concentration, photobleaching light dose, and photodynamic dose, are measured on individual cells (rat mammary cancer cell line, MTF7) using video laser fluorescence microscopy. Using the survival of the cells and the photodynamic dose given, a PDT protocol is proposed.

In Chapter 4, the measurement methods for the dye disappearances mentioned in Chapter 2 and 3 are expanded to a non-invasive method to determine indocyanine green, ICG, dye clearance from the liver. The study of ICG clearance in blood is clinically used for the estimation of hepatic function. Multiple blood samplings, however, subject the patients to mental and physical stress. Furthermore, although it is necessary with this method to correctly measure the blood sampling time after ICG injection, it is difficult to accurately measure this time in an actual test.. Thus, a measuring method without blood sampling has been desired. In this chapter, a description of an instrument for the non-invasive measurement of ICG clearance using an optical sensor attached to the fingertip is presented, and a calibration method before ICG injection is proposed to solve the problem of changing blood volume. Next, the results of the clinical evaluation are presented.

In Chapter 5, Monte Carlo simulation method and diffusion approximation method are proposed to examine the disappearance rate constants of ICG, the so called plasma disappearance rate from the liver. Over the past 10 years numerous theoretical models have been developed to describe the fluence distribution in turbid media such as biological tissues. These include Monte Carlo calculations (Wilson 1983, Prahl 1989), diffusion approximation derived from diffusion theory (Star 1989, Jacques 1987), adding doubling theory (Plass 1973, Prahl 1988), and combined models (Flock 1989). Monte Carlo calculations are considered as the most precise simulation method for steady state fluence distribution because various irradiation geometries can be treated, and the total number of photons increases the accuracy. The transmittance calculated by the diffusion theory and by the Monte Carlo method are both shown for the slab model to estimate the scattering effects for the plasma disappearance rate and retention rate of ICG from the liver.

Finally, in Chapter 6, the author summarizes the conclusion of this research and shows some research aspects in the future.

CHAPTER 2

PHOTOLABELING OF A DYE TO MEASURE THE DISTRIBUTION OF LIGHT

2.1 Introduction

Future applications of lasers and light in medicine and biology will increasingly involve reagents capable of photoactivation. One common application is photoactivation of adhesives or epoxies. One recent example is the photoactivated bifunctional linker which functions as a bonding agent for the purpose of anastomosis of cut tissue structures such as nerves, blood vessels, or tubular structures like the colon or vas deferens (Judy 1994).

The concept of photoactivation can include local photoactivation of a linking agent to achieve localized deposition of reagents. Local delivery of light might be used to affix a systemically delivered reagent at a particular tissue site via photolabeling. The affixed reagent could elicit a strong biological response (eg., inflammatory or immunological) which might kill the host if elicited systematically but which is systemically tolerated when localized at only one tissue site. Hence, a vigorous biological response can be targeted against one particular site selected by the irradiation. For example, a vigorous biological response stimulated in the area of suspected cancer might enable the body's defenses to recognize and attack cancer cells which under normal conditions are escaping detection.

Therefore, in this Chapter, as a model for photolabeling, the photolabeling of collagen gels with a fluorescent reagent called tetrabrominated rhodamine (TBR) (Shea and Hasan et al., 1989; Jacques and Hasan, 1992) is investigated . When a TBR molecule absorbs a photon (see Fig. 2.1A), one of its bromine atoms is displaced yielding a radical which can covalently attach to a protein such as collagen. The experiments involve Ar ion laser irradiation of collagen gels containing TBR. The affixed unbleached TBR was observed by fluorescence using an intensified video camera after removing all the unreacted TBR from the collagen gels with an overnight wash.

A

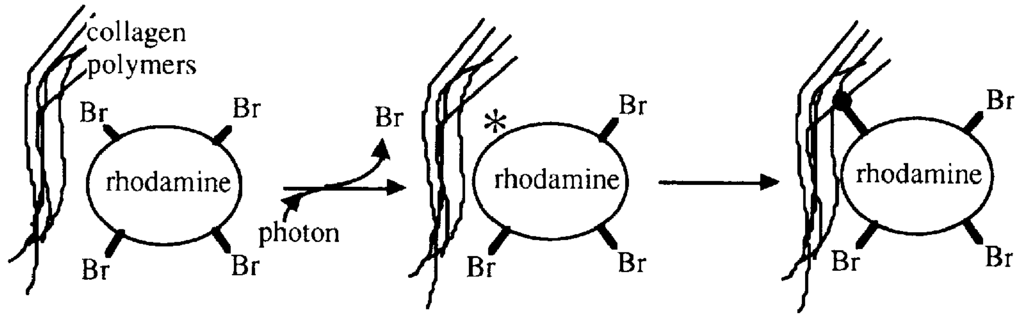

B

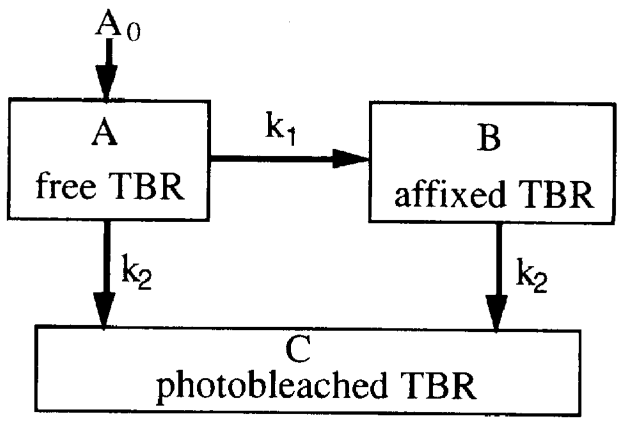

Figure 2.1: A: Schematic description of collagen photolabeling by TBR. Photon absorption causes debromination to produce a radical which binds covalently to the collagen polymer. B: Compartmental model for photolabeling and photobleaching. Free TBR (A) binds to collagen by photoactivation, debromination, and covalent bonding, yielding affixed TBR (B). Photobleaching of free and affixed TBR converts TBR into a nonfluorescent product (C).

The experiments addressed (1) the quantum efficiency of photolabeling, and (2) how dimethylsulfoxide (DMSO) might enhance the efficiency of photolabeling. The paper presents an analysis which yields photolabeling rates based on gel-affixed fluorescence despite losses due to photobleaching of affixed TBR by prolonged laser exposure. DMSO is known to disrupt the structured water surrounding macromolecules in solution (Szmant, 1971). The hypothesis was tested that DMSO enables the TBR molecule and its photoactivated radical to achieve closer association with the collagen molecules and thereby enhance covalent linkage.

2.1.1 Compartmental model for TBR photoaffinity labeling and photobleaching

The experiments in this paper can be described by the simple compartmental model of Fig. 2.1B. Initially, all the TBR is in compartment A which refers to free unbleached TBR that has not yet undergone either photolabeling or photobleaching. The initial concentration of TBR in the gel is A_o [M]. Laser irradiation causes binding of TBR onto the gel's collagen molecules. Compartment B refers to the affixed TBR that is still fluorescent. Compartment C refers to all TBR that has been converted to a nonfluorescent form (photobleaching).

The rate constant k_1 [s^{-1}] describes the rate of photolabeling collagen with TBR. The expression for k_1 in [s^{-1}] is:

$$k_1 = e_{tbr} E F_p \ln(10) 1000 b / L \tag{2.1}$$

The value of k_1 depends on the optical extinction coefficient of free TBR, e_{tbr} [cm^{-1} M^{-1}], the laser irradiance, E [W cm^{-2}], the quantum yield for photolabeling, F_p [dimensionless], which describes the probability of TBR fixation per photon absorbed by TBR, the number of photons per J at 488 nm, b [2.46e18 photons J^{-1}], and Avagadoro's number, L [6.02e23 $mole^{-1}$]. Since e is by convention defined using base 10, $e = -\log_{10}(T)/d$ where T is transmission and d is photon pathlength, the factor ln(10) is included in Eq. 2.1. Since there are 1000 cm^3 per liter, the factor 1000 is included. The above expression assumes that the concentration of collagen is in excess and not rate limiting for photolabeling, which may not be true. These experiments used 20 μM TBR in 4.5% collagen gels. Table 2.1 summarizes the parameters for a typical experiment.

Table 1: Parameters for a typical measurement (trial 5 in Fig. 5). This example is for a gel receiving a 110-s laser exposure that yields a maximum amount of affixed unbleached TBR.

Experiment:	**parameter**	**equation**	**value**	**units**
power	P		120e-3	W
beam diameter		2r	0.3	cm
beam area	Area	πr^2	0.071	cm^2
irradiance	E	P/Area	1.7	$W\ cm^{-2}$
exposure time	t		110	s
radiant exposure	H	Et	187	$J\ cm^{-2}$
gel thickness	d		500e-4	cm
extinction coefficient of TBR	e_{tbr}		6.25e4	$cm^{-1}\ M^{-1}$
initial concentration of TBR	A_o		20e-6	M
photons per J at 488 nm	b	l/hc	2.46e18	photons J^{-1}
Avogadoro's number	L		6.02e23	$mole^{-1}$
Observed:				
initial TBR	A_o			fluorescence lab units
affixed unbleached TBR	B(t)	Eq. 2.4b		fluorescence lab units
ratio	$B(t)/A_o$	Eq. 2.4b		dimensionless
Deduced by curve fitting:				
photolabeling rate constant	k_1	Eq. 2.1	0.0028	s^{-1}
photobleaching rate constant	k_2	Eq. 2.2	0.0077	s^{-1}
Calculated:				
ratio photolabeling/photobleaching	k_1/k_2		0.36	dimensionless
quantum efficiency photolabeling	f_p	Eq. 2.8	2.8e-6	dimensionless
quantum efficiency photobleaching	f_b	Eq. 2.9	7.7e-6	dimensionless
time of peak in B	t_{Bmax}	Eq. 6	110	s
peak in B/A_o	B_{max}/A_o	Eq. 7	0.11	dimensionless

The constant k_2 [s^{-1}] refers to the rate of photobleaching both free and affixed TBR. The value for k_2 depends on the quantum yield for photobleaching, F_b [dimensionless], which specifies the number of molecules of TBR photobleached per photon absorbed by TBR. The expression for k_2 is:

$$k_2 = e_{tbr} \, E \, F_b \ln(10) \, 1000 \, b / L \tag{2.2}$$

The differential equations describing the model in Fig. 1B are:

$$\frac{dA}{dt} = -A(k_1 + k_2) \tag{2.3a}$$

$$\frac{dB}{dt} = Ak_1 - Bk_2 \tag{2.3b}$$

$$\frac{dC}{dt} = (A + B) \, k_2 \tag{2.3c}$$

The solution of the above solutions are:

$$A = A_o \exp[-(k_1 + k_2)t] \tag{2.4a}$$

$$B = A_o (1 - \exp[-k_1 t]) \exp[-k_2 t] \tag{2.4b}$$

$$C = A_o (1 - \exp[-k_2 t]) \tag{2.4c}$$

The initial B increases linearly with exposure time:

$$B = A_o k_1 t \tag{2.5}$$

Figure 2.2 summarizes the above reactions using dimensionless parameters. Normalizing A, B, and C by the initial amount of free TBR (A_o) yields the dimensionless concentrations, A/A_o, B/A_o, and C/A_o. Multiplying time by the rate constant for photolabeling yields a dimensionless time unit, k_1t. A third dimensionless parameter is the ratio of the rate of photolabeling to the rate of photobleaching, k_1/k_2. Therefore, two dimensionless parameters $\{k_1t, k_1/k_2\}$ can describe the process of TBR photolabeling and photobleaching in a generic form. Figure 2.2 plots $\{A/A_o, B/A_o, C/A_o\}$ versus k_1t for various ratios of k_1/k_2.

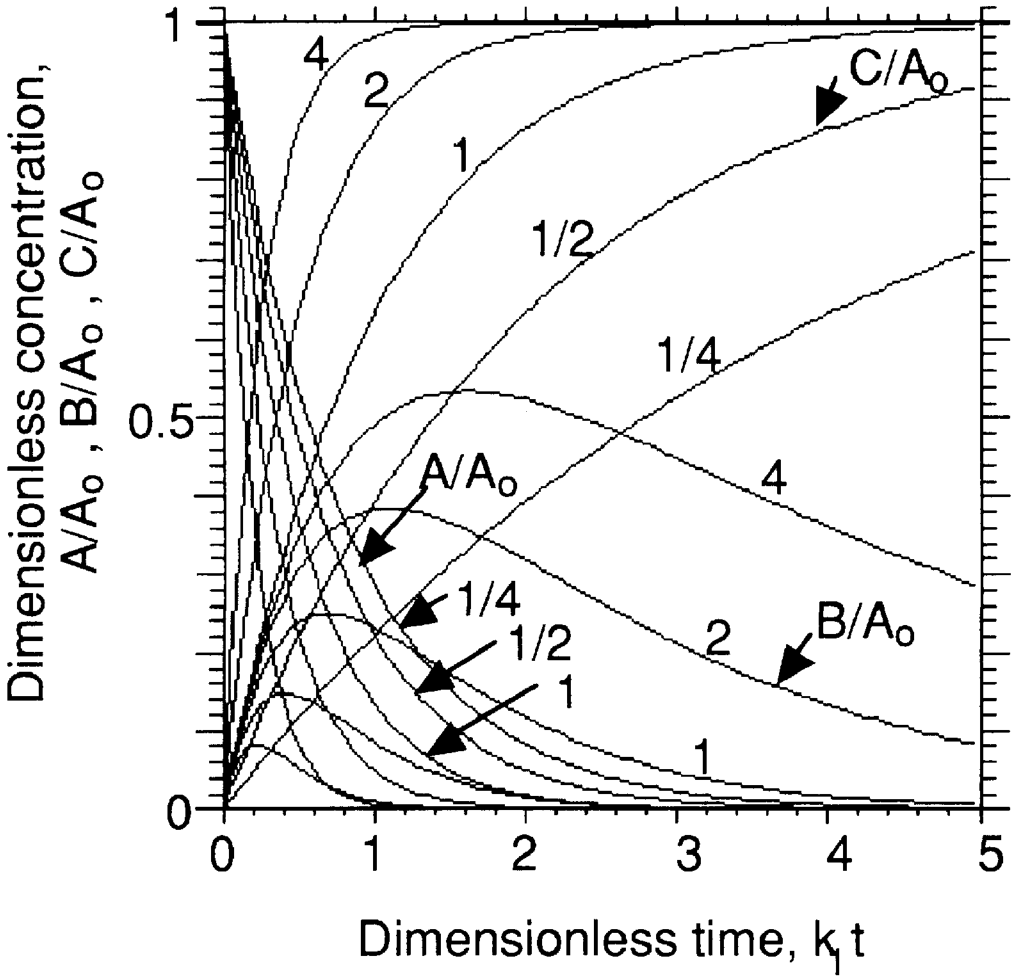

Figure 2.2: Dimensionless description of collagen photolabeling by TBR. The concentrations of free TBR in the gel (A), affixed unbleached TBR (B), and total photobleached TBR (C) are normalized by the initial free TBR concentration (A_o) and plotted as a function of dimensionless time (k_1t) where k_1 is the photolabeling rate constant [s^{-1}]. The family of curves indicate various ratios of photolabeling to photobleaching (k_1/k_2 = 1/4, 1/2, 1, 2, 4) [s^{-1}].

When photolabeling is much faster than photobleaching ($k_1/k_2 \geq 4$), B/A_o will achieve values exceeding 0.5 although a time delay occurs before achieving the maximum value. The ratio k_1/k_2 for the experiments reported here fall in the range of 0.1-0.6 (see Fig. 2.6c). The peak in affixed unbleached TBR occurs at t_{Bmax}:

$$t_{B_{max}} = \ln[\frac{k_1 + k_2}{k_2}] / k_1 \tag{2.6}$$

The peak value B_{max}/A_o is calculated by substituting $t_{B_{max}}$ for t in Eq. 2.4b:

$$B_{max}/A_o = \left(1 - \frac{k2}{k1 + k2}\right)\left(\frac{k2}{k1 + k2}\right)^{k2/k1} \tag{2.7}$$

The experiments reported in this paper involved measurement of the amount of affixed unbleached TBR (B) using TBR fluorescence after washing out all free TBR which had not photolabeled to the collagen gel. The measured data, B/A_o vs time, was fitted by Eq. 2.4b to specify the two rate parameters, k_1 and k_2.

2.1.2 Quantum yields for photolabeling and photobleaching

The quantum yield for photolabeling, F_p [dimensionless], is the probability of a TBR molecule binding to collagen after it has absorbed a photon. F_p is specified by the value of k_1 and expressed by solving Eq. 2.1 for F_p:

$$F_p = \frac{k_1\, L}{e_{tbr}\, E\, \ln(10)\, 1000\, b} = 0.0010\, k_1 \qquad (2.8)$$

The quantum yield for photobleaching, F_b [dimensionless], is the probability of TBR undergoing a transformation which causes loss of fluorescence after it has absorbed a photon. F_b is specified by the value of k_2 and expressed by solving Eq. 2.2 for F_b:

$$F_b = \frac{k_2\, L}{e_{tbr}\, E\, \ln(10)\, 1000\, b} = 0.0010\, k_2 \qquad (2.9)$$

The factor $L/(e_{tbr}\ E\ \ln(10)\ 1000\ b)$ equaled 0.0010 [s] for these experiments.

2.2 Materials and methods

2.2.1 Chemicals

Tetrabrominated rhodamine (TBR) was prepared by T. Hasan (Hasan 1989). The TBR was stored in the dark at -26 °C at a stock concentration of 400 μM in methanol (absorption coefficient μ_a = 25 cm^{-1}). Five experiments (experiment one, trials 1-4; experiment two) were conducted with one batch of TBR. A second batch of TBR was used for experiment one, trials 5-6. DMSO (dimethylsulfoxide, Cat.#D-5879, Sigma Chemical Inc.) was used both in preparing some of the gels (0-40% DMSO by weight) and in the washing solution (5% DMSO) for removal of unreacted TBR. The collagen was cell-cultured-tested gelatin from porcine skin (Cat. #G-2500, Sigma Chemical Inc.).

2.2.2 Collagen gel phantom

The collagen gel phantom solution was prepared using the recipe in Table 2. About 1/2 ml of the prepared collagen gel solution was placed in a 33-mm-diameter petri dish to make a thin film (gel thickness = 500 μm). Actual thicknesses were determined by transmission measurements at 488 nm using an integrating sphere (typical transmission was 0.95 through the air/ plastic/air/gel/plastic/air aminate and increased to 0.98 if the gel was replaced by water). Preparation was conducted under a red safelight and gelatin stock was kept warm (~45°C) to facilitate mixing. Several gels were mixed and poured to provide sufficient room for replicative trials of each experimental condition. Each gel was divided into 16 sites, and each experimental condition used 8 sites. Data were plotted as the mean ± standard deviation (n = 8 gel sites). After solidification, the petri dishes were covered, sealed with Parafilm™ to avoid dehydration, and kept inverted to avoid condensation on the dish cover. When the experiment was first tried, the petri dishes holding the gels were not covered and sealed, and during the experiment the gel underwent dessication. Therefore, the first two trials are labeled as "dessicated" and the last four trials with properly sealed gels are labeled as "no dessication". In experiment two, gels with different concentrations of DMSO were prepared to study how DMSO would influence TBR photolabeling.

Table 2: Recipe for preparation of collagen gel.

Component stock	**gel with**	**DMSO**	**gel without**	**DMSO**
	% volume stock	**final amount**	**% volume stock**	**final amount**
μ_a TBR = 25 cm^{-1} (400 μM)	5	μ_a TBR = 1.25 (20 μM)	5	μ_a TBR = 1.25 (20 μM)
DMSO	25	25% DMSO	0	0% DMSO
10% collagen gel solution	45	4.5% collagen	45	4.5% collagen
water	25	65.5%	50	90.5%

2.2.3 Laser exposure

The 120-mW 488-nm beam from an Ar ion laser (Ion Laser Technology, Salt Lake City, Utah) was used to irradiate the gel to achieve photolabeling. The laser beam was focused through a quartz lens into a 300-μm-diameter quartz optical fiber, and the terminal end of the optical fiber was imaged via a 10X objective lens to form a 3.0-mm-diameter flat-field circular spot on the gel. The irradiance was 1.7 W/cm^2. The collagen-TBR gels were exposed to the Ar ion laser beam using a range of exposure times to yield radiant exposures of 0-800 J/cm^2. The beam was delivered through the inverted bottom of the dish with sealed cover as shown in Fig. 2.3. The gel was inverted to allow irradiation from the bottom side of the plate which avoided any vapor condensation interfering with the exposure. Experiments were conducted at room temperature (25° C).

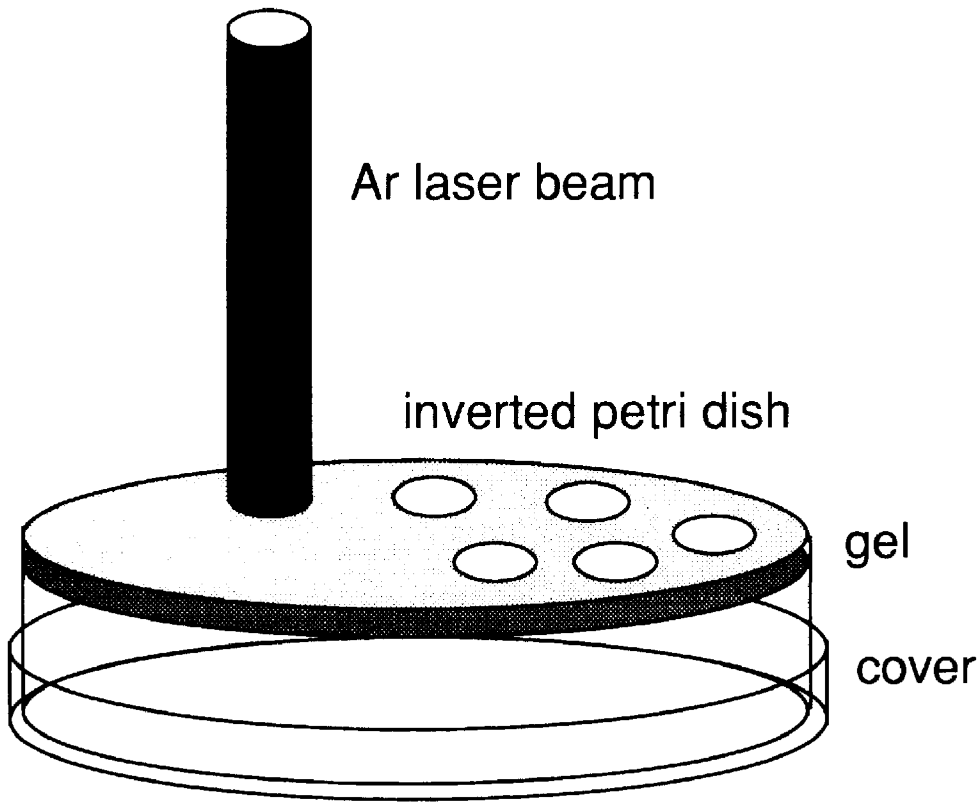

Figure 2.3 Exposure of 0.5-mm collagen-TBR film to Ar ion laser radiation.

2.2.4 Washing out unreacted TBR

After irradiation, the gel was placed in a 1000-ml volume of water with 5% DMSO and stirred overnight. This procedure washed out the unreacted free TBR. Only a slight background amount of TBR remained in the unexposed area of the gel, although the residual amount increased at higher DMSO concentrations.

2.2.5 Video fluorescence measurement

Prior to laser exposure, the TBR fluorescence at each site of the gels was measured using a low-intensity video fluorescence imaging system. The gels were illuminated with a low-intensity expanded flat-field beam (0.8 mW/cm^2) of Ar laser radiation in order to excite TBR fluorescence. A video camera (Dage-MTI, Inc.) with an image intensifier (VS2525, Videoscope International, Ltd.) and a dissection scope (Olympus, Inc.) provided video images which were acquired by computer (MacIntosh) using image processing software (Image 1.22, NIH). Fluorescence intensity was measured by counting the mean pixel value within the intended site of laser irradiation. The initial fluorescence was proportional to the initial free TBR concentration, A_o. After laser exposure and after removal of the unreacted TBR by overnight washing, the gel fluorescence of each site was again determined. This fluorescence score was proportional to the affixed unbleached TBR, B. The ratio B/A_o was calculated and recorded, which canceled any perturbations caused by minor site-to-site variations in the gel thickness.

2.3 Results

Figure 2.4 illustrates the fluorescence image of a typical gel which has received multiple sites of laser exposure. As the laser exposure increases, the amount of photolabeling increases. However, at still higher exposures the affixed TBR is photobleached. Two experiments were conducted.

2.3.1 Experiment 1: Kinetics of photolabeling and photobleaching

The first experiment measured the yield of affixed unbleached TBR as a function of laser exposure time. The results established the rate constants for photolabeling and photobleaching of TBR on collagen gels. Experiments were conducted using gels with or without 25% DMSO. Gel sites were irradiated for various times at a constant irradiance, then the unreacted TBR was removed from the gel by an overnight washing. The fluorescence video system documented affixed fluorescent TBR as a function of time, B(t).

Figure 2.5 plots the results of a typical gel experiment (trial 5). The affixed unbleached TBR is plotted as a function of the laser exposure time [s] at an irradiance of 1.7 W/cm^2. The TBR is expressed as the normalized value of affixed fluorescence/initial

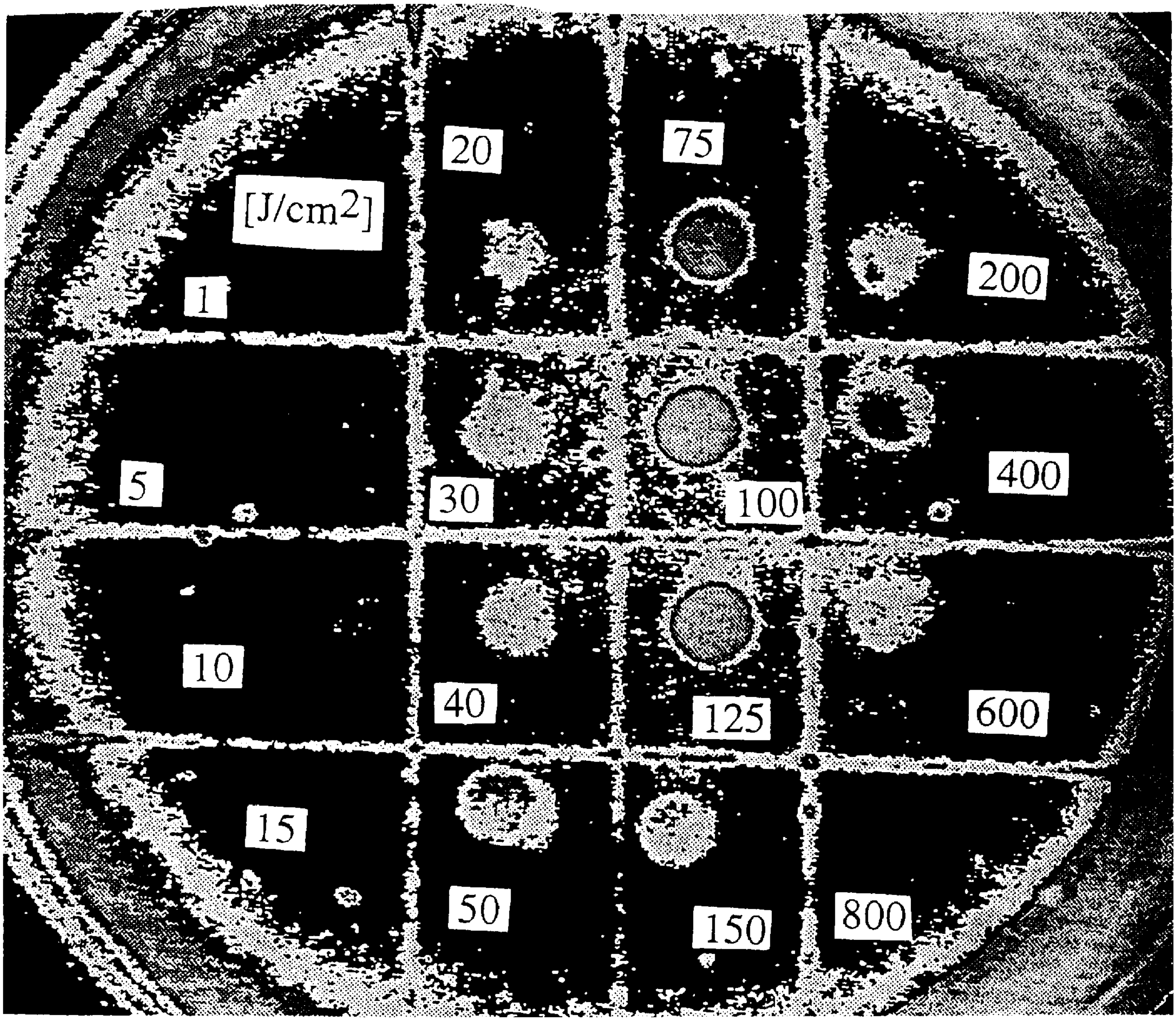

Figure 2.4: Video image of a gel with regions of affixed TBR observable as fluorescence after washing unreacted TBR from the gel. The gel was divided into 16 sites which received Ar ion laser exposure at 1.7 W/cm^2 for various times in a 3-mm-diameter flat-field beam. As the radiant exposure [J/cm^2] increased, the amount of affixed TBR increased to a maximum than dropped as continued exposure caused photobleaching.

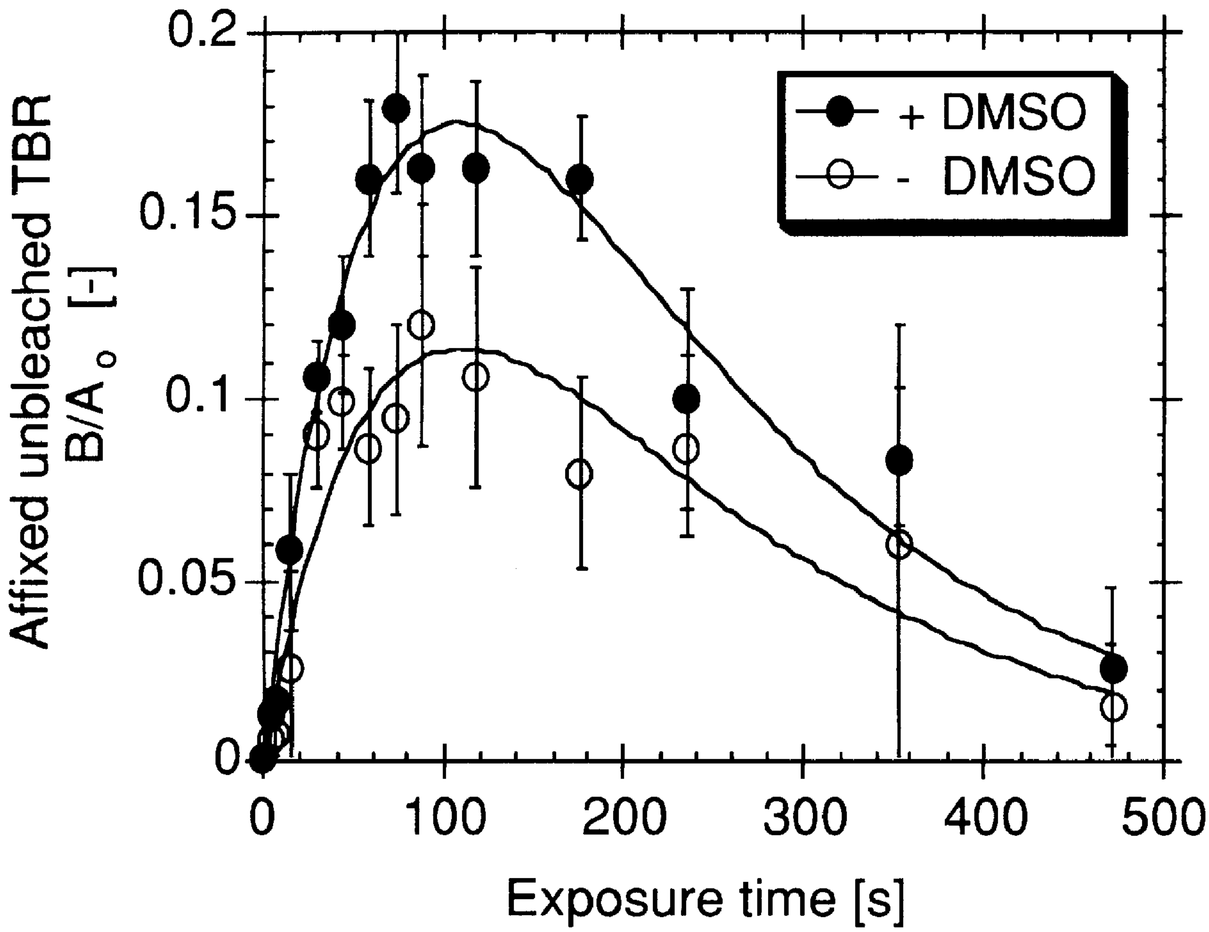

Figure 2.5: Typical experiment (trial 5 in Fig. 6). The affixed unbleached TBR (B) was normalized by the initial amount of free TBR (A_o) and plotted versus the exposure time at 1.7 W/cm^2 irradiance. The initial increase in B was rapid, peaked at about 100 s, then decreased as photobleaching of the TBR occurred. The inclusion of 25% DMSO in the gel caused an increase in the maximum value of B/A_o. (Mean ± standard deviation , n = 8 gel sites per radiant exposure.)

fluorescence, B/A_o, based on the gel fluorescence before and after laser exposure. The solid lines indicate the fit of Eq. 4b to the data. The maximum fluorescence intensity occurred after about 110 s or 187 J/cm^2. At higher exposures, photobleaching caused gel-affixed fluorescence to decrease. The addition of DMSO (25% by volume) increased the maximum yield of photolabeled TBR, B_{max}/A_o, by 55% from 0.11 to 0.17. The rate constants (k_1, k_2) were (0.0028 s^{-1}, 0.0077 s^{-1}) without DMSO and (0.0045 s^{-1}, 0.0072 s^{-1}) with DMSO for the experimental case of 20e-6 M TBR concentration.

Figure 2.6 summarizes the results for the 6 trials of experiment 1 conducted on separate occasions with freshly prepared solutions and materials. Figure 6A shows that the photolabeling constant, k_1, was greater in the presence of 25% DMSO than without DMSO. Figure 2.6B shows no significant effect of DMSO on the photobleaching rate. Figure 6C shows the ratio k_1/k_2 was in the range 0.1-0.6 because photobleaching was dominant over photolabeling. During trials 1-2, the gels were not sealed which allowed dessication. Trials 3-6 were properly sealed. Trials 1-4 used the first batch of synthesized TBR. Trials 5-6 used a second batch of TBR. In trials 1-2 DMSO was more effective in enhancing photolabling than in trials 3-4 because in the dessicated gels the DMSO acted as a solvent. Comparison of trials 3-4 vs trials 5-6 indicate that the second batch of TBR yielded more efficient photolabeling than the first TBR batch, although no explanation is offered. The mean ± standard deviation (n = 4 trials) of (k_1, k_2) for trials 3-6 with no gel dessication were (.0012 ± .0004 [s^{-1}], .0103 ± .0044 [s^{-1}]) without DMSO and (.0025 ± .0007 [s^{-1}], .0096 ± .0039 [s^{-1}]) with 25% DMSO.

(See next page)

Figure 2.6: Summary of experiment 1 (six trials). (A) Photolabeling constant (k_1). (B) Photobleaching constant (k_2). (C) Ratio k_1/k_2. Trials 1 and 2 were unsealed and the gel suffered dessication. Trials 3-6 were sealed and there was no dessication. Trials 1-4 used one batch of TBR. Trials 5-6 used a second batch that was apparently more effective. The presence of 25% DMSO increased k_1 relative to gels without DMSO, but had no significant effect on photobleaching.

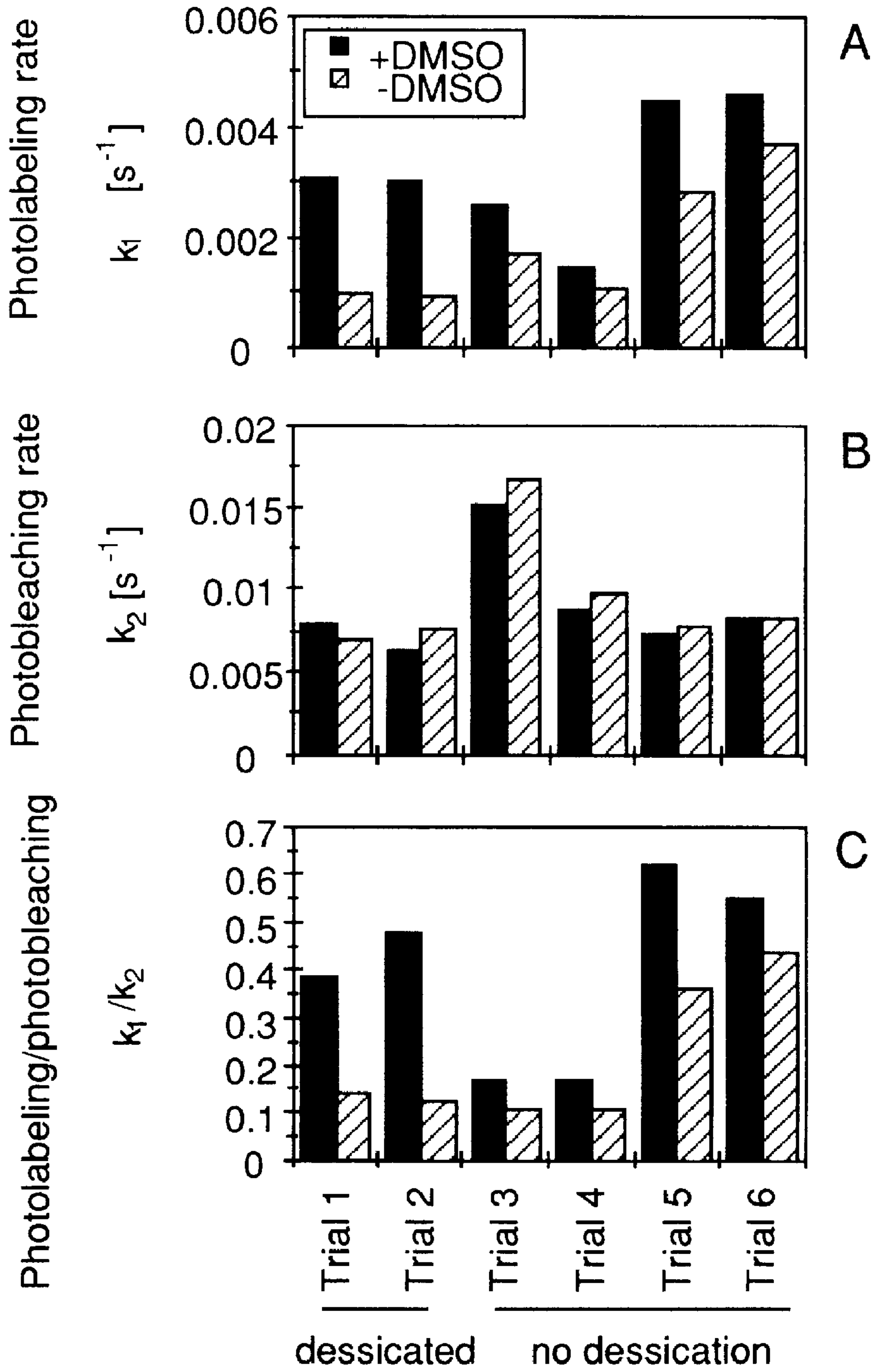

A
B
C
+DMSO
-DMSO
Photolabeling rate
k_1 [s^{-1}]
0.006
0.004
0.002
0
Photobleaching rate
k_2 [s^{-1}]
0.02
0.015
0.01
0.005
0
Photolabeling/photobleaching
k_1/k_2
0.7
0.6
0.5
0.4
0.3
0.2
0.1
0
Trial 1
Trial 2
Trial 3
Trial 4
Trial 5
Trial 6
dessicated
no dessication

2.3.2 Experiment 2: Dependence of photolabeling on DMSO

The second experiment studied how varying the DMSO concentration in the gel affected the net yield of affixed unbleached TBR. At a constant laser exposure (100 J/cm^2), the amount of DMSO in the gel was varied.

Figure 2.7 shows the affixed TBR fluorescence versus the concentration of DMSO (% by volume) in the gel. The yield of photolabeled TBR (B/A_o) increased rapidly with added DMSO. The presence of 10% DMSO increased the yield of TBR fluorescence about 2-fold. At 25% DMSO, the yield of TBR reached a maximum of about 2.4-fold enhancement. At 40% DMSO, the photolabeling dropped slightly below the maximum. The experiment was conducted using the first batch of TBR, so the peak B/A_o value was lower than that attained in trial 5 shown in Fig. 5 which used the second batch of TBR. No explanation for the differences in photolabeling efficiency of the two TBR batches has yet been determined.

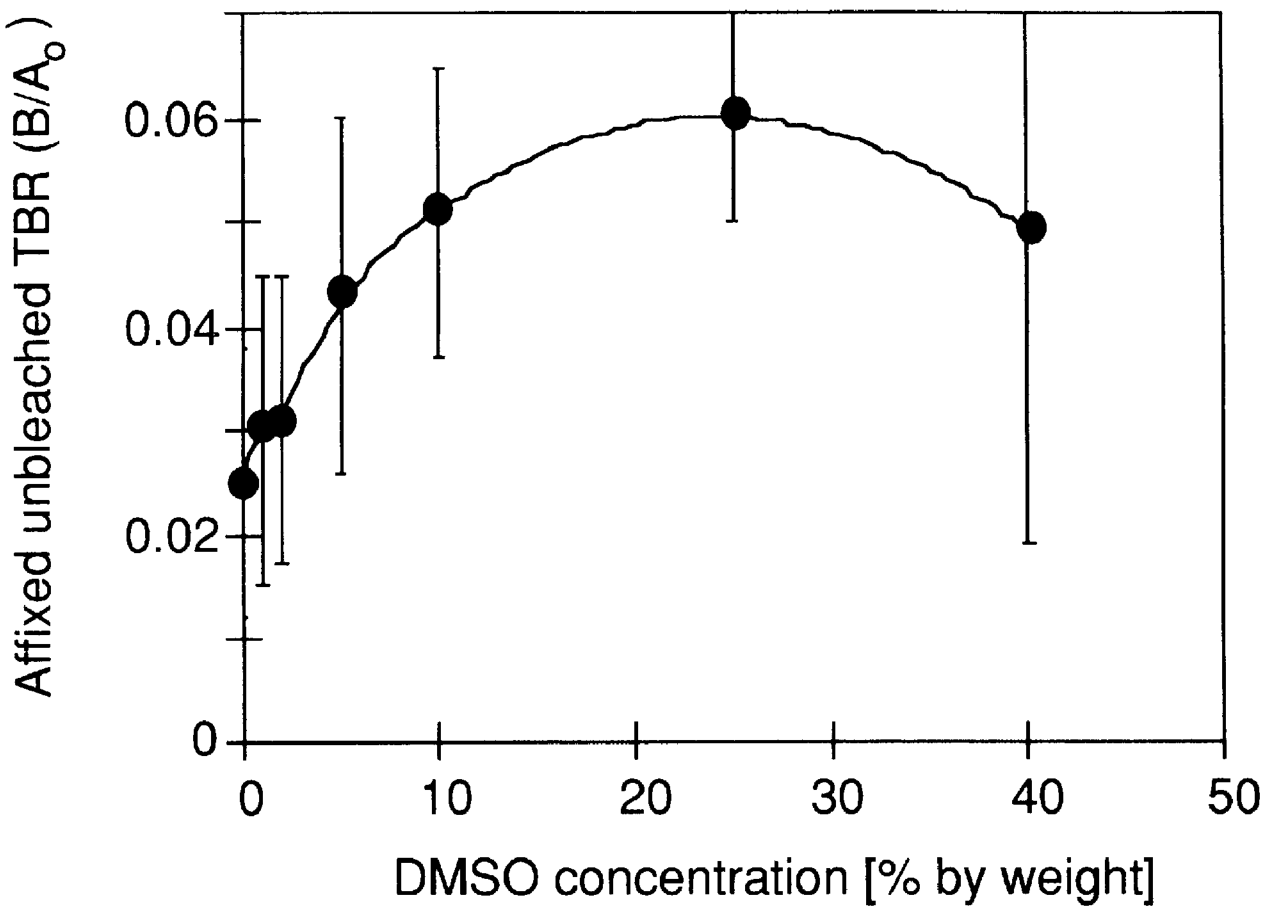

Figure 2.7: The effect of DMSO concentration on photolabeling of collagen gel by TBR. Laser exposure was constant at 100 J/cm^2. (Mean ± standard deviation , n = 8 gel sites per DMSO concentration.)

2.4 Discussion

The use of a fluorescence reagent when conducting photolabeling studies can be very convenient. The amount of affixed reagent is easily assayed by a rapid noninvasive optical measurement, even in *in vivo* animal or cell culture models. But photobleaching due to prolonged laser exposure can complicate such a fluorescence assay.

The first experiment illustrated how a compartmental model can describe the photolabeling process even when photobleaching is a factor. The maximum amount of observable affixed fluorescent reagent, B_{max}, occurs at a specific time, t_{Bmax}. In the case of any photolabeling reagent which also undergoes photodestruction, similar kinetics are expected.

The second experiment indicated the ability of DMSO to enhance photolabeling. DMSO is known to break the water structure surrounding proteins by replacing the hydrogen bonds of water molecules. The results of this paper suggest that DMSO has replaced some of the water around collagen thereby disrupting the water structure and permitting TBR to move closer to the collagen for more efficient bonding upon photoactivation by debromination. The results have shown that 10% DMSO will double the amount of affixed TBR and 25% DMSO achieves a 2.4-fold maximum enhancement of photolabeling.

2.5 Conclusion

The fixation of a photosensitive reagent, tetrabrominated rhodamine (TBR), onto collagen gels was studied as a model for photolabeling biological tissues with medical reagents. The kinetics of photolabeling process was modeled using a compartmental model. Parameters of the model were determined by experiments on tissue simulated gel films. It is suggested that DMSO has replaced some of the water around collagen thereby disrupting the water structure and permitting TBR to move closer to the collagen for more efficient bonding upon photoactivation by debromination.

The results showed that photolabeling is a powerful way to estimate the optical propagation in tissue and also the compartmental analysis tells us the quantitative information about the photochemical processes.

CHAPTER 3

PHOTOBLEACHING OF A DYE FOR CANCER CELLS

3.1 Introduction

In Chapter 2, we discussed the photolabeling process of a fluorescence dye, TBR, to know the propagation of laser in collagen-gel-films as a tissue phantom. Photolabeling process is usually combined with photobleaching process mentioned in the previous chapter, but it is still essential to measure the concentration of a dye especially for photo-dynamic therapy, PDT, as a method to treat cancers. In this Chapter, PDT for cells using δ-aminolevulenic acid (ALA) is studied. Administration of ALA, the metabolic precursor for the heme synthetic pathway, can induce the accumulation of protoporphyrin IX (PPIX) in cells (Malik 1987, Ades 1990). Such ALA-induced PPIX is currently under investigation in many centers for the purpose of photodynamic therapy (PDT) which is a light-activated chemotherapy for cancer and other indications (Dimitrios 1990, Bedwell 1993, Loh 1992). PPIX serves as a photosensitizing agent for PDT. Establishing effective protocols requires a knowledge of the local concentration of PPIX in a targeted cell culture or tumor. Because PPIX photobleaches during irradiation, the photobleaching light dose constant is also required to predict the photodynamic dose experienced by the target tissue.

This Capter reports the distribution of two parameters in a putatively homogeneous population of cancer cells in culture: (A) the initial concentration of PPIX in cells, C_0 [µg/cell], and (B) the photobleaching light dose constant, H_{pb} [J/cm^2]. The measurements involved quantitative video fluorescence microscopy of single cells during prolonged irradiation. The C_0 and H_b were used to predict the photodynamic dose, D_{PDT} photons absorbed by PPIX/g cells or [ph/g], that would be attained in each cell after complete photobleaching of all PPIX. A colony formation study of cell survival after individual irradiation of single cells via the microscope is presented. The techniques allows specification of the individualized D_{PDT} of cells which were successfully killed and of cells which survived the treatment.

3.1.1 Photobleaching and fluorescence

Photobleaching of PPIX in a cell is expected to follow first-order kinetics with respect to the radiant exposure, H [J/cm^2], of the single cell. Assume that the initial distribution of PPIX is uniform in a cell at a concentration C_0 [µg/ml]. The PPIX in the cell undergoes photodestruction, called photobleaching, and C_0 decays as:

$$C(t) = C_0 \exp(-t/\tau) \tag{3.1}$$

where

$$\tau = \frac{Hpb}{E} \qquad (3.2)$$

The photobleaching time constant, τ [s], depends on the irradiance of the photobleaching light, E [W/cm^2], and the photobleaching dose constant, H_{pb} [J/cm^2]. In our experiments, we measured t at a specified E and deduced H_b.

3.1.2 The photodynamic dose

The photodynamic dose is defined as the number of photons absorbed by PPIX per g of cells, D_{PDT} [ph/g] (Patterson 1990). This parameter indicates the number of excited state PPIX molecules generated per unit mass of cells and is proportional to the amount of singlet oxygen (putatively) generated which contributes to oxidative damage leading to cell death. The D_{PDT} parameter provides an important dosimetric measure for comparison of the efficiency of different photosensitizers to achieve photodynamic action. Patterson, Wilson, and Graff (1990) illustrated that D_{PDT} was a constant value independent of the wavelength of irradiation in their study of PDT-induced necrosis in rat livers (Patterson 1990).

The D_{PDT} depends on the irradiance, E, and the concentration of PPIX, C_0, but this product must be integrated over the exposure time, T, since photobleaching depletes the PPIX according to Eq. 1. The integral is:

$$D_{PDT} = \frac{e}{br} \int_0^T C_0 \exp(-t/t)\, E\, dt$$

$$= \frac{eC_0Et}{br} (1 - \exp(-t/t)) = \frac{eC_0H_b}{br} (1 - \exp(-H/H_b)) \qquad (3.3)$$

where e is the extinction coefficient of PPIX at 488 nm [0.023cm^{-1}/(μg/ml)], b is the energy per photon at 488 nm [4.07e-19 J/photon], r is the density of a cell [~1.0 g/ml], C(t) is the PPIX concentration as it photobleaches, E is the irradiance [W/cm^2], T is the exposure time [s], H is the radiant exposure equal to ET [J/cm^2], and H_b [J/cm^2] is the photobleaching exposure that reduces C(t) by a factor 1/e.

If the PPIX is completely photobleached ($t \gg \tau$, or $H \gg H_b$), the maximum D_{PDT} obtained is proportional to the product C_0H_b.

$$D_{PDT} \text{ for complete photobleaching} = \frac{eC_0H_b}{br} \qquad (3.4)$$

This study measured both C_0 and H_b for individual cells. The maximum D_{PDT} obtainable in individual cells was calculated using Eq. 3.4. In the colony formation study, cells received a radiant exposure of either 20 or 300 J/cm^2 and Eq. 3.3 was used to calculate the true D_{PDT} of each cell.

3.2 Materials and methods

3.2.1 Cell cultures

The cancer cell line used in the study was MTF7, cloned from a 7,12-dimethyl-benz[a]-anthracene-induced rat mammary adenocarcinoma (Tomasovic 1983), courtesy of Dr. Stephen P. Tomasovic, Department of Tumor Biology, M. D. Anderson Cancer Center. The cells were grown in a-MEM (Alpha-modified, Minimum Essential Eagle, Sigma Chemical Co., St. Louis, MO) supplemented with 10% fetal bovine serum (HyClone Laboratories Inc., Logan, UT) in monolayers in petri dishes.

ALA (Sigma Chemical Co., St.Louis, MO) was introduced into the culture media at various concentrations, specified later, and the cells were incubated as monolayers on petri dishes for 24 hr. The cell concentration in culture at harvest was ~0.7e6 cells per petri dish which was not confluent. At the time of the PPIX assay, the cells were loosened from 3 petri dishes by the addition of trypsin to the medium (0.25%) and incubated for 5 min at 37 °C. The loosened cells were resuspended in phosphate buffer saline (PBS), centrifuged, and resuspended in 1 ml of PBS, to yield 2e6 cells/ml.

Two cell preparations were studied: (Preparation A) Twenty μl of the cell suspension (40e3 cells) were placed on a glass slide with a cover slip for fluorescence microscopy. (Preparation B) Cell digests were prepared by placing 1 ml of PBS containing 2e6 cells into 2 ml of Scintigest (Fischer Scientific), a solvent/digestant which yielded a clear solution after 18 hr. The cell digest was placed in a polystyrene cuvette for bulk fluorescence measurements using the OMA.

3.2.2 Fluorescence assay for PPIX

Two fluorescence measurements were conducted. (A) Video fluorescence microscopy (F_{vid}) measured single cells. (B) An optical-fiber fluorescence spectrophotometer (F_{oma}) measured cell digests. Comparisons of the two measurements together with calibration experiments using F_{oma} enabled calibration of the video (F_{vid}).

3.2.3 Fluorescence microscopy

The level of PPIX in single cells was assayed by the fluorescence microscopy system shown in Fig. 3.1. The measurement system used a 488-nm argon ion laser (Coherent, Inc., model Innova 90) delivered through an inverted microscope (Zeiss, Inc., model Axiovert 405M) to excite PPIX fluorescence in individual cells. Fluorescence was observed through a 580-nm long-pass filter with an intensified CCD camera (Video Scope International Inc., VS2525 intensifier, CCD200E camera) and recorded by video tape (Panasonic, AG-6300). The laser was delivered through an optical fiber whose termination was imaged through the microscope to yield a uniform-field beam in the image plane. The irradiance of the laser was 5.8 W/cm^2 and the beam was 180 µm in diameter. The recorded fluorescence images were sent to a personal computer (MacIntosh) for acquisition and analysis using an image processing system (Image, NIH). The measurements were recorded as a porphyrin fluorescence score.

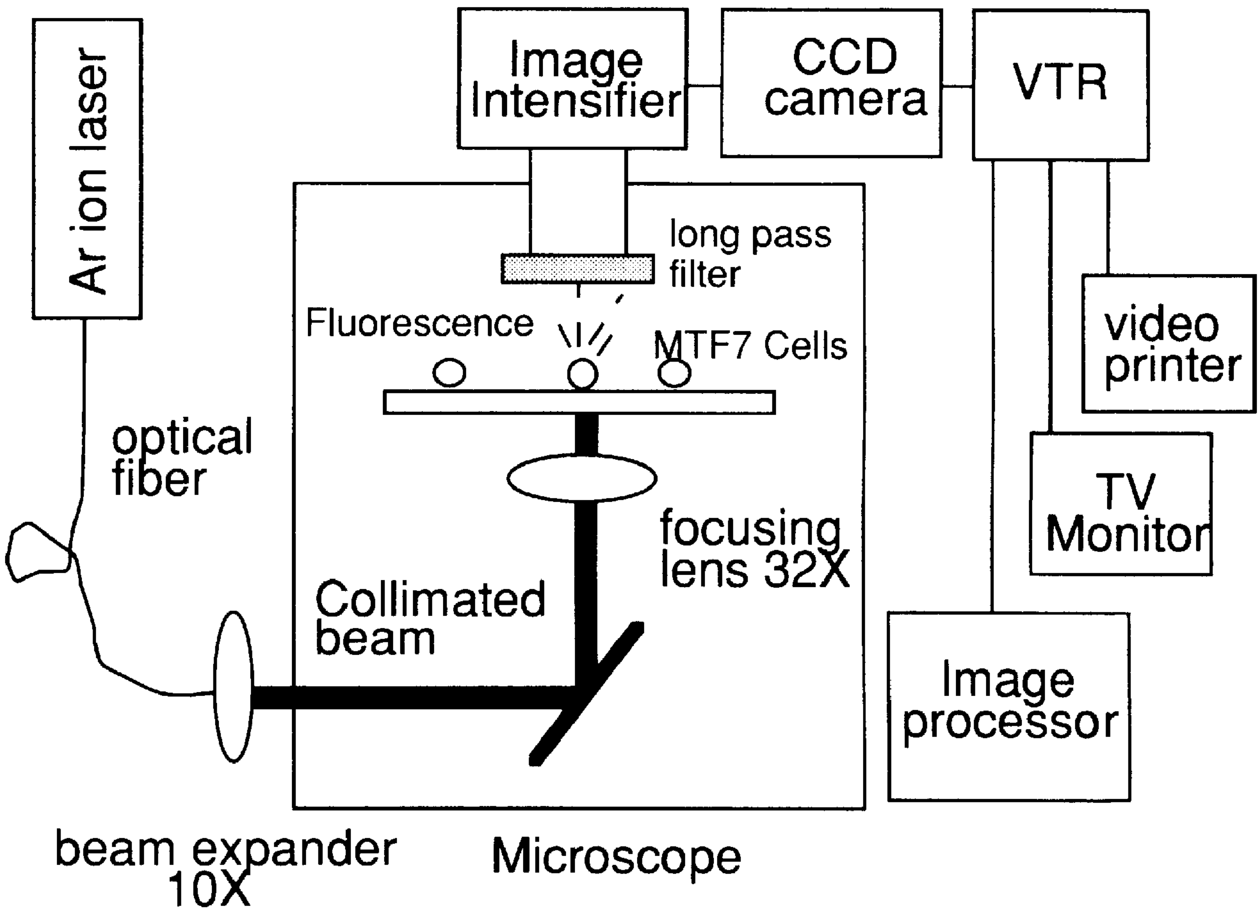

Figure 3.1: Fluorescence microscopy apparatus. An argon ion laser (488 nm) excited cellular PPIX fluorescence and an intensified CCD camera viewed the emission through a 580-nm long-pass filter.

A porphyrin fluorescence score, F_{vid} in laboratory units called [video units/cell], was defined by the following:

$$F_{vid} = A\ N\ F_{camera} \tag{3.5}$$

where A was the cell cross-sectional area [μm^2/cell], N was the number of pixels per unit area in the image processing system [2.13 pixels/μm^2], and F_{camera} was the fluorescence intensity in laboratory units [video units/pixel].

3.2.4 Cell digest fluorescence measurements (OMA)

Measurements of PPIX in cell digests utilized a fluorescence spectrophotometer. The system used a nitrogen-dye laser (Laser Science, Inc., Newton, MA) at 420 nm delivered through an optical fiber to excite cell fluorescence and an optical mutichannel analyzer (OMA) (Princeton Instruments, Inc., Trenton, NJ) to detect fluorescence. The same 600-µm-core-diameter fiber both delivered excitation and collected emission. The fiber was placed against the side of a polystyrene cuvette containing a cell digest (preparation B). The porphyrin fluorescence score (F_{oma}) was determined by integrating the area under the fluorescence curve between 600-750 nm and normalizing by a standard reference which was the peak fluorescence of a fluorescein standard solution routinely measured to account for day-to-day variation in the system. The background F_{oma} for cells grown without PPIX was subtracted from all F_{oma}

measurements, and all values of F_{oma} reported here have undergone such a background subtraction.

3.2.5 Calibration experiments

3.2.5.1 Microscope calibration

Cells were incubated for 24 hr in various concentrations of ALA to yield a range of PPIX levels. Individual cells (preparation A) were measured with the video camera (F_{vid}). A cell digest (preparation B) was measured with the fluorescence spectrophotometer (F_{oma}). Figure 3.2 plots the PPIX fluorescence in the cell digest (F_{oma}) vs the PPIX fluorescence of the same cells measured by fluorescence microscopy (F_{vid}). The relationship was linear:

$$F_{oma} = A + c_{vid}^{oma} F_{vid} \tag{3.6}$$

where A is the y-intercept (10.5 [oma]), and c_{vid}^{oma} is the slope (0.00044 [oma/(video units/cell)]).

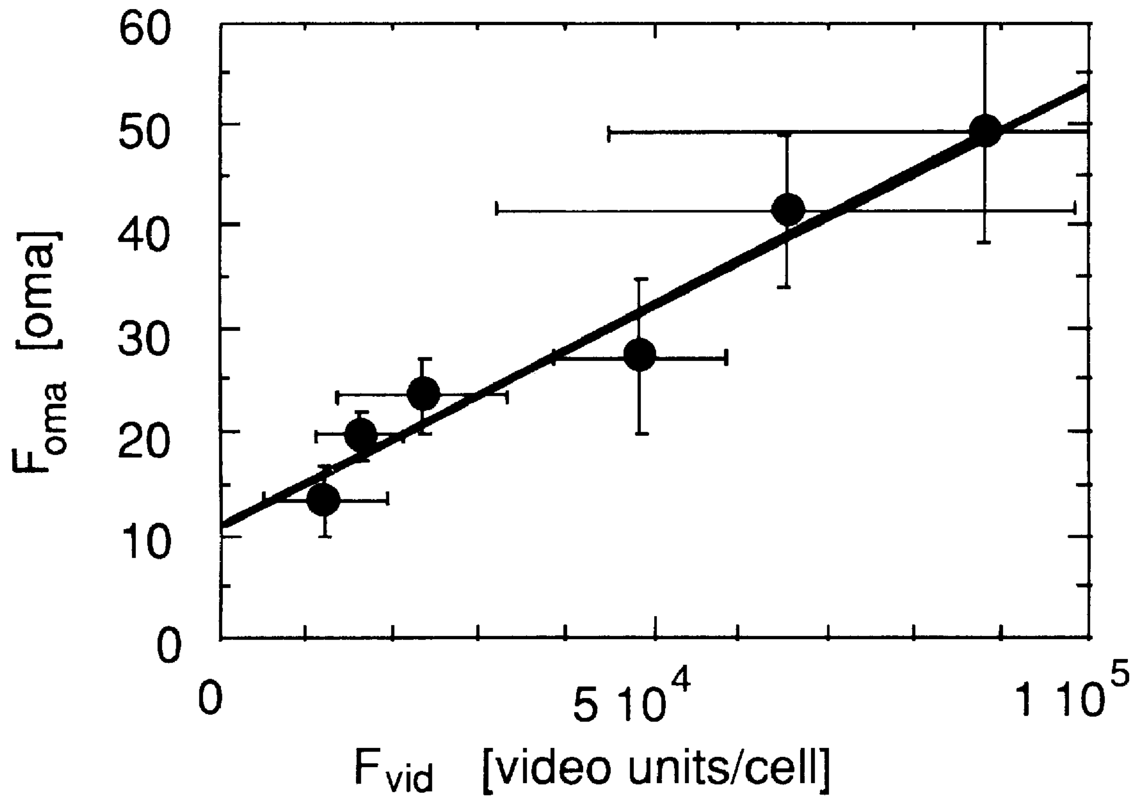

Figure 3.2: Calibration curve relating the PPIX fluorescence measured by spectrometer in a cell digest (F_{oma}) vs the fluorescence measured in cells by video microscopy (F_{vid}).

3.2.5.2 OMA calibration

In a second experiment, cells not grown in ALA were prepared as a cell digest (preparation B). Known amounts of PPIX [μg] were added to the digest and F_{oma} measurements made. Figure 3.3 plots the fluorescence of a cell digest (F_{oma}) vs the amount of added PPIX [μg], yielding a linear relation with a slope, c^{oma}_{PPIX}, equal 249 [oma/μg PPIX].

Combining the above two calibration experiments, the relationship between a video measurement, F_{vid}, and the cellular PPIX concentration, C_0 [μg/ml], was:

$$C_0 = \frac{A + F_{vid}\, c^{oma}_{video}}{c^{oma}_{PPIX}\, N\, V_{cell}} = \frac{10.5 + F_{vid}\,(0.00044)}{(2e6)(249)V_{cell}} \qquad (3.7)$$

N was the number of cells in the cell digest (2e6 cells). V_{cell} was the volume of the particular cell measured [ml/cell]. Each cell's volume (V) was estimated based on the cell's diameter observed in the two-dimensional image acquired by the camera, assuming a spherical shape for the nonadherent cell. Experimentally, the C_0 values were specified by Eq. 3.7 from the F_{vid} values at the start of irradiation before significant photobleaching could occur. For example, if the F_{vid} was 50,000 video units/cell, and the V_{cell} was 2.6e-8 ml/cell, then the C_0 was 2.5 μg/ml within the cell.

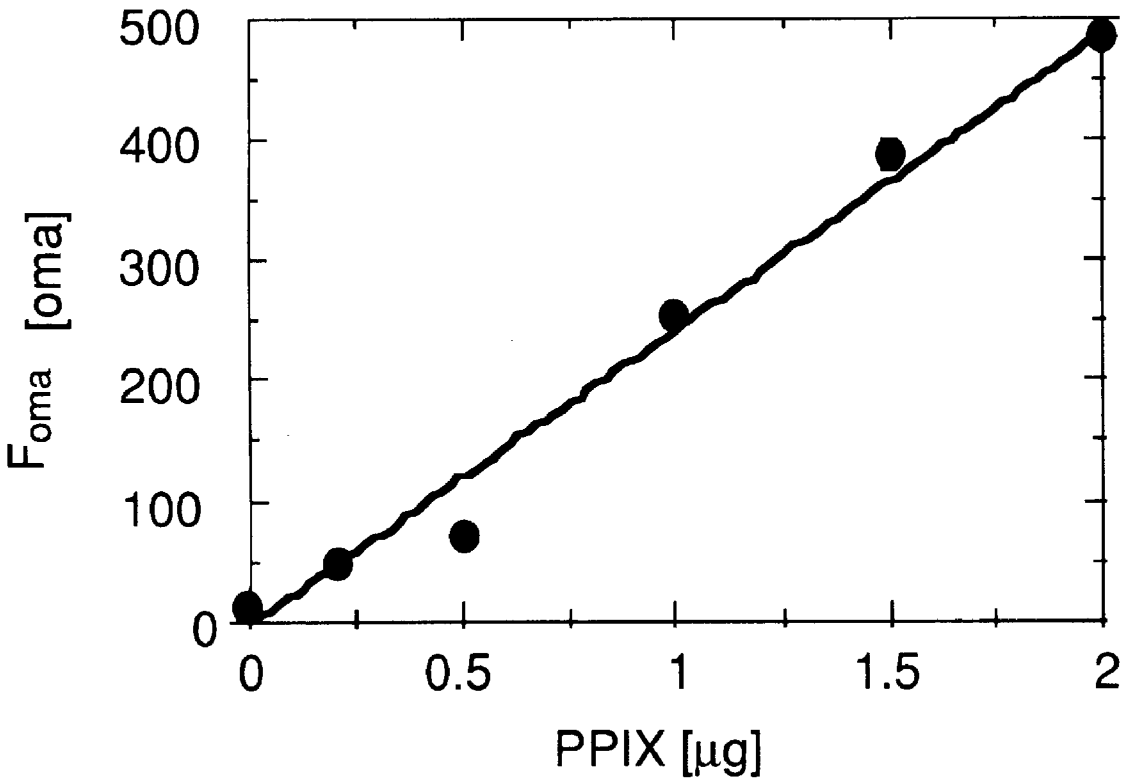

Figure 3.3: Calibration curve for PPIX fluorescence in a cell digest (F_{oma}) vs the µg of PPIX added to the cell digest.

3.2.6 Colony formation

Cells in mid-log phase growth were plated onto petri dishes at a low density, about 200 cells per plate, and incubated in 200 μg/ml ALA for 24 hours. The plates had grids drawn on their bottom surface to facilitate identification of cells at a given position. A sampling of cells was observed with the inverted fluorescence microscope during the individual irradiation of single cells. 36 cells were given 20 J/cm^2 and 81 cells were given 300 J/cm^2. Video recordings measured the initial C_0 of each cell and the decay due to photobleaching. Because the petri dish imposed a relatively high amount of autofluorescence, only the initial photobleaching could be documented, however the values of H_b obtained were similar to the previous study of cells on glass. In this study, the mean ± standard deviation for H_{pb} was 102 ± 51 [J/cm^2]. Because the cells were adherent to the petri dish, the V_{cell} was calculated by assuming a hemispherical shape. The D_{PDT} of each cell was calculated using Eq. 3.3, accounting for the radiant exposure utilized (20 or 300 J/cm^2). After exposure, the cells were incubated for 3 days, then scored for signs of successful colony formation.

3.3 Results

3.3.1. Experimental data

When one observes a fluorescent cell by eye through the microscope, the total fluorescence is distributed over the cell cross-sectional area, A [μm^2], in the field of view to yield a particular brightness, which can be expressed as F_{vid}/A [pixel units/μm^2]. Figure 3.4 plots F_{vid}/A versus A. Cells not incubated in ALA (n = 16) had a mean value of 8.7, and cells incubated in ALA (n = 124) had a mean value of 107.

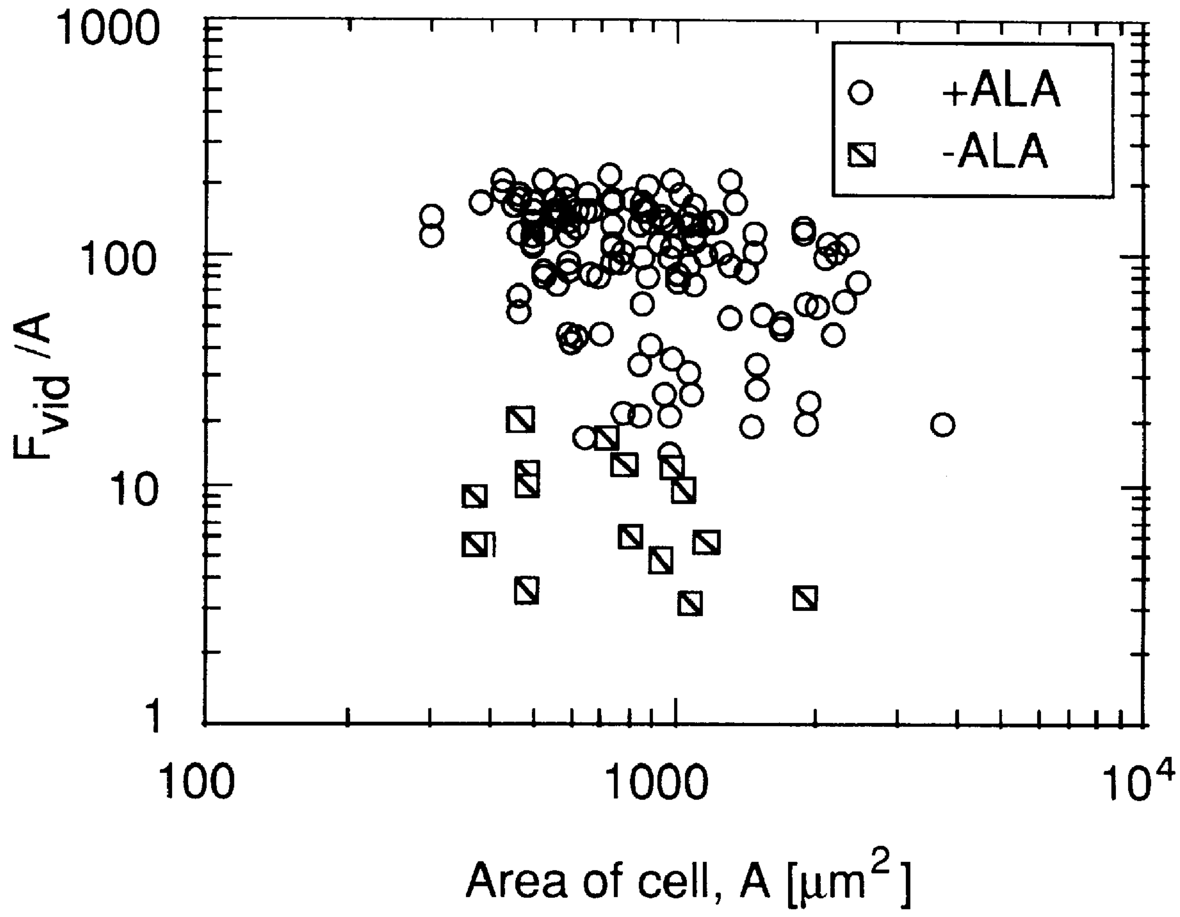

Figure 3.4: The brightness of cellular fluorescence as seen by the eye with a microscope through 580-nm long-pass filter, quantified by the video camera as F_{vid}/A. The total fluorescence (F_{vid}) was distributed over the area of the cell (A). Data are plotted versus cell area. Incubation of cells in ALA (+ALA) yielded about 10-fold brighter fluorescence than cells grown without ALA (-ALA).

3.3.2 Histograms

Figure 3.5 shows the histograms of the initial PPIX concentration, C_0 [μg/ml], the photobleaching light dose, H_{pb} [J/cm^2], and the photodynamic dose, D_{PDT} [ph/g]. The mean (and range) of C_0 was 6.0 (1-15) μg/ml. Control cells not grown in 5ALA showed 0.52 [μg/ml] (not shown). Assuming these C_0 values were primarily due to PPIX and that background non-porphyrin auto-fluorescence in the 600-750 nm range was negligible, the amount of PPIX induced by 5ALA was about ten times the amount of endogenous PPIX in cells. The H_b was 135 (25-300) J/cm^2, which was surprisingly variable. The maximum D_{PDT} obtained after complete photobleaching of PPIX was calculated to be 5.2e19 (3e18-2e20) ph/g.

(See next page)

Figure 3.5: Histograms of (top) the initial concentration of PPIX, (middle) the photobleaching light dose constant, and (bottom) the photodynamic dose achieved by complete photobleaching of the cellular PPIX.

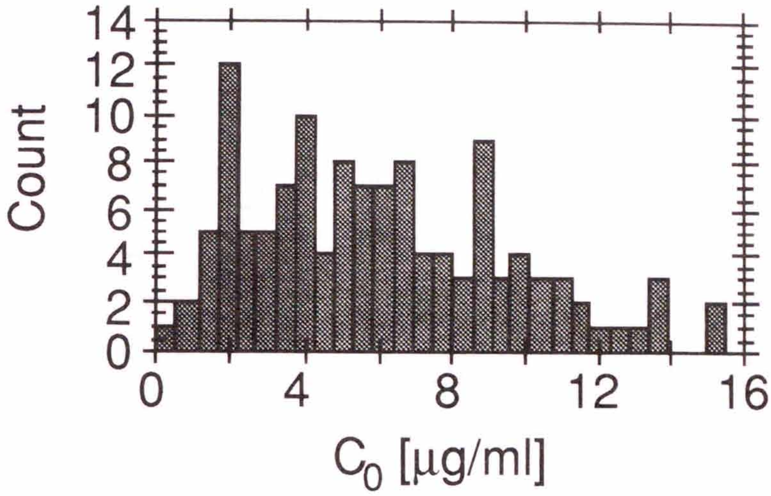
Count
C0 [μg/ml]
0
2
4
6
8
10
12
14
16

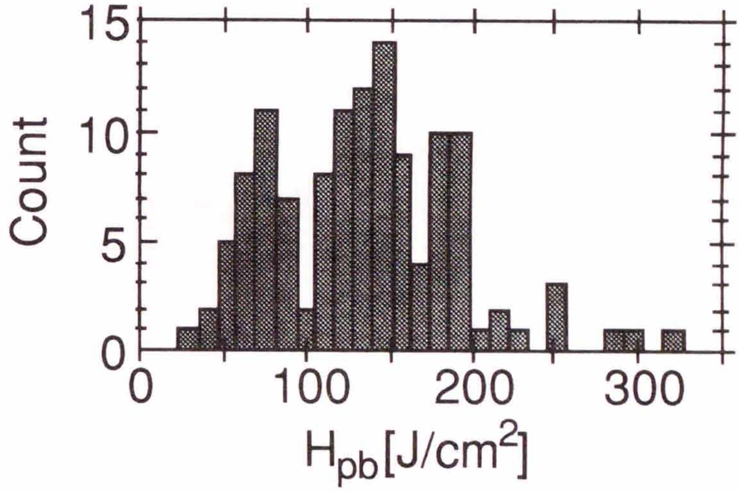
Count
Hpb [J/cm2]
0
5
10
15
100
200
300

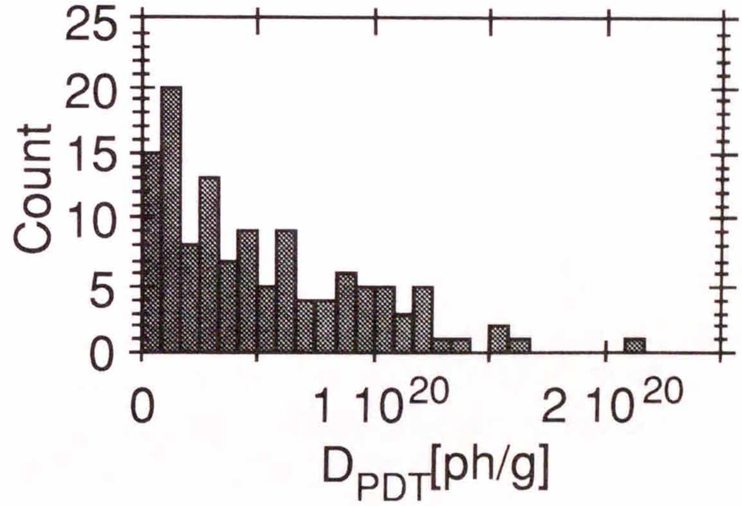
Count
DPDT [ph/g]
0
5
10
15
20
25
1 10^20
2 10^20

Figure 3.6 shows the correlation between D_{PDT} and C_0, and the mean values of 5.2e19 ph/g and 6.0 µg/ml, respectively. The slope should be $\varepsilon H p_b/br$ or 8.7e18 (ph/g)/(µg/ml), as indicated by the solid line. The noise derives from variations in the experimentally measured H_b and the measured cell size used to estimate V_{cell} for calculation of C_0. The slope overestimates the data at low C_0 and underestimates the data at high C_0. The most striking aspect of the data is that this apparently homogeneous population of cells is behaving so heterogeneously with respect to PPIX accumulation and photobleaching.

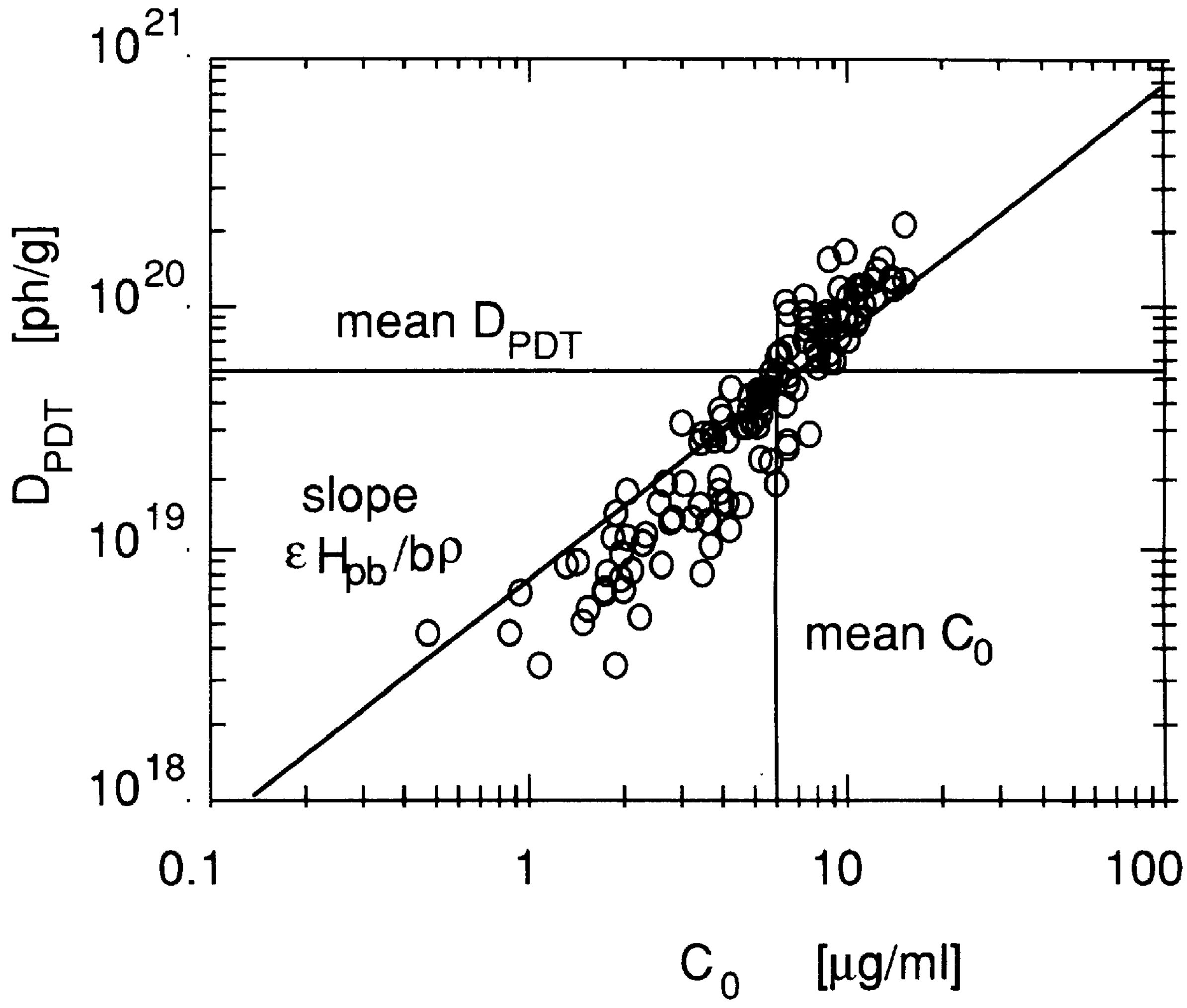

Figure 3.6: Correlation of the maximum photodynamic dose (D_{PDT}) and the PPIX concentration in cells (C_0), with mean values 5.2e19 ph/g and 6 µg/ml, respectively. The slope should be $\varepsilon H_{pb}/br$, as described in Eq. 3.4.

3.3.3 Bleb formation

Figure 3.7 shows bleb formation, an indicator for photodynamic damage to cell membranes, in a cell after 350 J/cm^2 of laser exposure which was sufficient to cause nearly complete photobleaching of PPIX. Before the cell was exposed to the laser (Fig. 3.7a), there was no bleb. After exposure (Fig. 3.7b), the cell displayed a bleb at the 10 o'clock position. The bleb itself had no PPIX fluorescence.

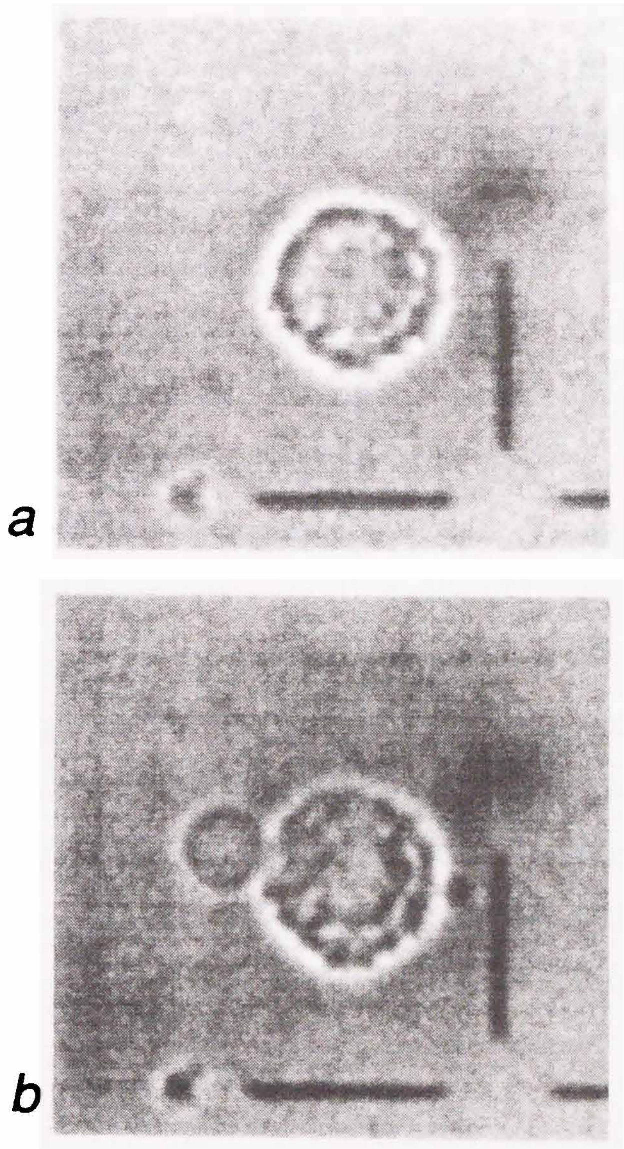

Figure 3.7: Bleb formation in a cell exposed to laser radiation that completely photobleaches the cellular PPIX. (a) Cell before exposure. (b) Cell after exposure.

3.3.4 Colony formation

The results of the colony formation study are shown in Fig. 8. The calculated D_{PDT} for each cell is specified by the y-axis. In the study, 36 cells received 20 J/cm^2 and 81 cells received 300 J/cm^2 radiant exposure. After 3 days incubation, the occurrence of cell colonies was scored. The cells killed by PDT and those that survived are compared. The D_{PDT} obtained with 300 J/cm^2 was higher than with 20 J/cm^2, of course, and the rate of colony formation was lower at the high exposure than the low exposure, 3/81 (3.7%) vs 8/36 (22%), respectively. However, there was not a sharp threshold value of D_{PDT} which demarcated death from survival. Some dosages were as low as 1e18 but achieved cell kill. Other dosages were as high as 3e19 and failed to kill. The threshold D_{PDT} for killing falls in the range of 1e18-3e19. Within that range, most cells were killed but a significant fraction survived. Our work continues to explore celling killing vs survival at low D_{PDT} exposures.

3.4 Discussion

The concept of a threshold photodynamic dose was studied by Patterson, Wilson, and Graff (1990) using another photosensitizer, aluminum chlorosulphonated phthalocyanine (AlSPC) (Patterson

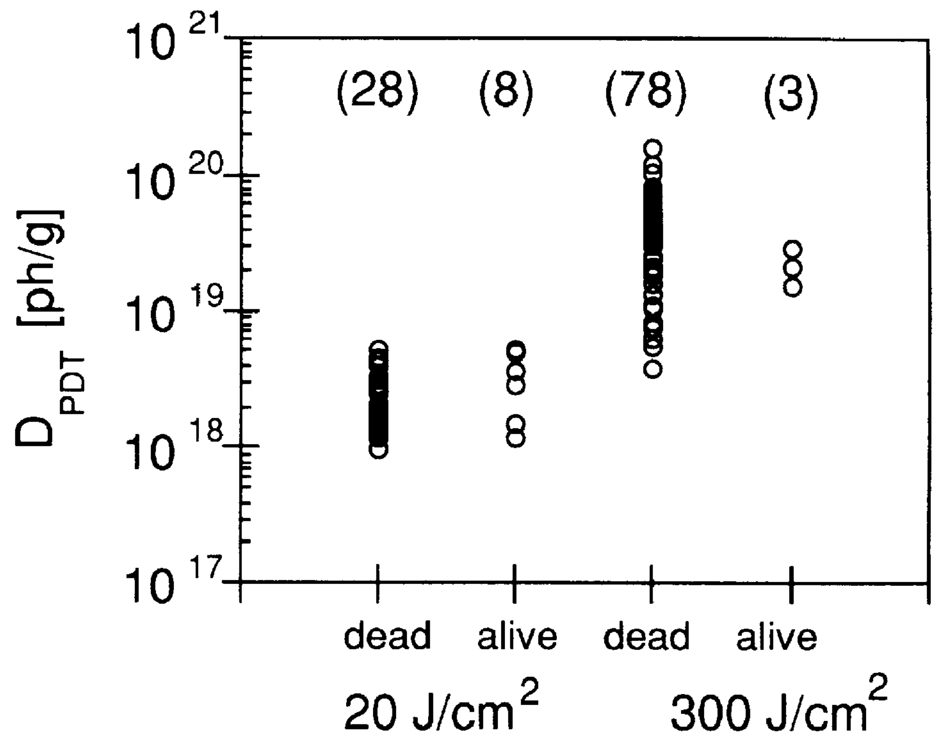

Figure 3.8: Colony formation study. Cells individually received light exposure while video recordings documented C_0 and H_{pb}, allowing the D_{PDT} of individual cells to be calculated. Cells received either 20 or 300 J/cm^2 at 488 nm wavelength. The D_{PDT} values of cells that died and cells that survived to form colonies are shown. The lowest dose that killed was about 1e18 ph/g and the highest dose that failed to kill was 3e19 ph/g.

1990). They reported a threshold D_{PDT} of 3.8e19 for achieving necrosis in rat liver. These authors also estimated a threshold D_{PDT} of 8.6e17 for the photosensitizer PhotofrinII to achieve necrosis in human tumors, based on the work of Potter (Potter 1989). Recently, Chen et al. (1994) have reported a threshold D_{PDT} of 4.0e19 for PhotofrinII to achieve necrosis in dog prostate (Chen 1994). The estimated range for a threshold D_{PDT} of 1e18-3e19 reported for PPIX in this paper is consistent with the values for PhotofrinII. PPIX appears relatively efficient in achieving photodynamic killing of cells.

3.5 Conclusions

The analysis for PDT in cells is discussed. The amount of PPIX attained by the cells ranged between 1-15 µg/g cells, with a mean value of 6.0 µg/g cells. The photobleaching dose constant was 135 ± 56 J/cm^2. The photodynamic dose obtainable after complete photobleaching ranged between 2e18-5e19 with a mean value of 5.2e19 [photons absorbed by PPIX per g cells]. A colony formation study indicated that the threshold D_{PDT} required for cell killing fell in the range of 1e18-3e19.

CHAPTER 4

METHOD FOR MEASURING DYE DILUTION IN BLOOD AND ITS CLINICAL EVALUATION

4.1 Introduction

So far, the fluorescence of dyes are applied for measuring the concentration of the dye or the propagation of light. In Chapter 3, *in vitro* measurement of the dye concentration in a single cells based on a fluorescence microscopy was discussed. In addition to using fluorescence, transmitted lights through an object can be applied for measureing a dye *in vitro* or *in vivo*. In this chapter, we intend to apply the fluorescence method mentioned previous Chapters for transmittance measurement using indocyanine green dye, ICG, *in vivo* which has done conventionally *in vitro*. Indocyanine green (ICG)(Fox 1957) is widely used as a sensitive tracer for the estimation of hepatic function. The principal characteristics of ICG are very low toxicity, confinement to the vascular compartment because of binding to plasma proteins, rapid excretion from liver and presence of an absorption maximum near the isobestic point of hemoglobin (Landsman 1978). In particular, the study of ICG clearance rate in blood is one of the best methods for evaluating hepatic diseases such as liver cirrhosis (Takaki 1967, Howard 1967). In 1969 a reference method using ICG clearance rate was established by the Japanese Society of Gastroenterology (Namihisa 1969). Clinically, multiple blood samplings have been necessary to determine the values for the ICG tests (Namihisa 1963) such as plasma disappearance rate and 15-minute retention ratio after intravenous ICG injection which subject the patients to mental and physical stress. Furthermore, although it is necessary with this method to correctly measure the blood sampling time after the ICG injection, it is difficult to accurately measure this time in an actual test. Accordingly, a measuring method without blood sampling has been desired. A non-invasive method was tried to developed by using a spectrophotometric measurement of the ear lobe (Yokosuka 1986). Although the spectrophotometric method called the ear piece method, was developed as an ICG test without blood sampling, fitting and stabilization of the optical sensor presents some difficulties. To eliminate those problems, a new method by measuring the transmittance light through the tip of the index finger before and after ICG injection was proposed. This paper describes this newly developed instrument and its evaluation.

4.1.1 Optical characteristics of ICG

After its introduction, ICG soon came into general use for dye dilution tests. The principal advantage of the dye used *in vivo* was the presence of an absorption maximum near the isobestic point of hemoglobin. Absorption spectra of ICG and hemoglobin are shown in Figure 4.1. In human tissue, hemoglobin, which is contained in the blood, is the major absorbance factor. The spectrum of hemoglobin changes depending on its oxygen saturation but the absorption maximum of ICG is close to this isobestic point. Therefore, ICG concentration can be measured *in vivo* at 805nm unaffected by hemoglobin oxygen saturation.

4.1.2 ICG test using blood sampling

Clinically, the ICG tests are standard methods for the patients with hepatic diseases. The tests are conducted with the patient in a supine position in a fasting state. Blood is sampled before intravenous ICG injection . In general, one blood sampling is performed as a reference. After intravenous injection of ICG, blood sampling is also performed three times after of 5, 10 and 15 minutes. Blood plasma is separated upon coagulation of a blood clot so that the absorbance at 805 nm is measured through a spectrophotometer to obtain ICG concentration values in the blood plasma from a previously obtained line, corresponding to ICG concentration in blood vs. absorbance. These ICG concentration values in the blood plasma are plotted on the ordinate of semilogalithmic scale with time recorded on the abscissa because the disappearance is expected to follow first-order kinetics with respect to the time after ICG injection.

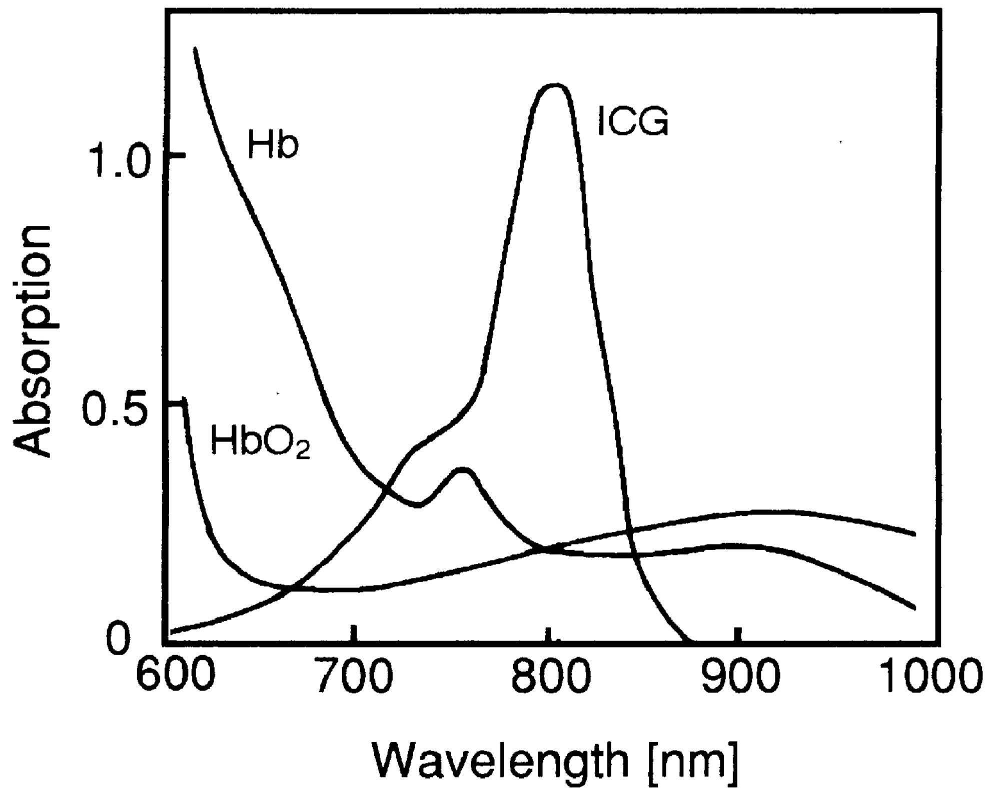

Figure 4.1: Absorption spectra of hemoglobin and indocyanine green(ICG). ICG has its peak absorbance at 805 nm in protein solution. This wavelength is the isobestic point of hemoglobin. There is no ICG absorbance at more than 900 nm.

The plasma disappearance rate, K [min^{-1}] is calculated using the formula;

$$C_t = C_o \cdot \exp(-K \cdot t) \tag{4.1}$$

$$K = \frac{\log C_o - \log C_t}{t} \tag{4.2}$$

where t is time in minutes after ICG injection, C_{15} is ICG concentration in the blood plasma after 15 minutes and C_o is the calculated initial ICG concentration in the plasma, when the ICG dosage is 0.5 mg per kilogram of body weight. The 15 minute retention ratio R_{15} as a clinical estimation value of hepatic function is defined as follows;

$$R_{15} = \frac{C_{15}}{C_o} \cdot 100 \ [\%], \tag{4.3}$$

Usually, C_o in Eq.(4.3) is clinically determined to be 1.00.

4.1.3 Prototype of continuous method

A dichromatic ear densitometer measured the difference of the transmittance at 800 and 900 nm to derive the ICG concentration (S_g) as follows;

$$S_g = K_g \cdot (\log T_{800} - \log T_{900}), \tag{4.4}$$

where K_g is a constant that depends on the ICG absorption coefficient. T_{800} and T_{900} are the transmittances at 800 and 900 nm respectively. However, the output measured by Eq.(4.4) fluctuates due to influence from the changing blood volume at the measuring site. Considering this problem, the following relationship was derived (Aoyagi 1975),

$$S_g = \{\frac{\log(I_{800}/T_{800})}{\log(I_{900}/T_{900})} - K_b\} \cdot K_g \tag{4.5}$$

where K_b is the constant value of the bloodless state. In this method, before ICG injection, the ear lobe is pressed by the ear piece of the dichromatic ear densitometer in order to obtain measurements of I_{800} and I_{900}, the bloodless transmittances at 800 and 900 nm. Next, measurements of the normal blood-containing state is obtained by releasing the pressure on the earlobe and measuring T_{800} and T_{900}, the transmittances at the same two wavelengths. In actuality, the values I_{800}, I_{900} and K_b are treated as constant values. Using with the two conditions described above as references, T_{800} and T_{900}, transmittances of the former normal state after ICG injection, are measured to calculate S_g value. As a result, it is reported that the influence of the change of blood volume can be compensated for using this method. However, to obtain correct ICG disappearance curve, common problems that exist in conventional ear densitometry must be addressed:

a) because using a Xenon or halogen lamp as a light source heats the ear piece, more than 20 minutes idling time is necessary to stabilize

the densitometer, but since the ear lobe is warmed, the blood volume gradually increases and hemoglobin is oxygenated,
b) the ear piece frequently slips down because of its weight, but the blood volume decreases when it is attached tightly to prevent slipping, and
c) to get enough absorbance of ICG from the ear lobe, heating or some other method is necessary to increase blood flow.

4.2 Materials and methods

4.2.1 The newly developed measuring algorithm

Relationship between the transmittances at 810 and 940 nm before injection of ICG are expressed as:

$$\log T_{810} = A_{810} + A_{810}^{ICG} \tag{4.6}$$

$$\log T_{940} = A_{940} \tag{4.7}$$

where T_{810} and T_{940}: transmittance through the fingertip at 810 and 940 nm, A_{810} and A_{940}: are the absorbances of tissue and blood at 810 and 940 nm.

Extracting absorbance information on ICG is done by seeking A_{810}^{ICG} from Eq.(4.6). However, changes in the ICG concentration contain a large noise component. This is because the absorbance of the blood varies greatly with changes in the blood flow volume in the end of the finger, thus causing the noise component. In order to remove this noise component using this apparatus, a wavelength at which ICG does not have absorbance is used as shown in Eq.(4.7). The relationship between the absorptions of the two wavelengths by the blood and tissue is shown by the following equation before the intravenous injection of ICG, which establishes calibration constants between the wavelengths of the transmitted light.

$$\log T_{810} = a \cdot \log T_{940} + b \tag{4.8}$$

Here, a and b are constants decided by the least square method at the time calibration is actually performed. In practice, Eq.(4.8) is obtained by greatly changing the amount of blood flow in the end of the finger by raising and lowering the hand to which the ICG sensor has been attached. After intravenous injection of ICG, the calibration data from Eq.(4.8) is used to calculate the blood and tissue absorbance of Eq.(4.6) from Eq.(4.7), and the ICG absorbance A_{810}^{ICG} is calculated by subtracting this. Therefore, the ICG concentration, Sg, is defined as :

$$S\,g = \{\log T_{810} - (a \cdot \log T_{940} + b)\} \cdot K g \tag{4.9}$$

The value S g is constantly zero before the injection of ICG, if the blood volume changes, and is defined as the base line of the disappearance curve. The time change of Sg is expressed as:

$$S_g = S_o \cdot \exp(-K \cdot t) \quad (4.10)$$

where t represents the elapsed time in minutes after injection of ICG, and S_o represents the Sg value at t =0. Further, R_{15} is expressed as:

$$R_{15} = \exp(-K \cdot 15) \quad (4.11)$$

4.2.2 Optical sensor

The ICG clearance meter has light emitting diodes (LEDs) that emit at 810 and 940 nm, and a near-infrared silicon photodiode used as a photodetector. The 810 nm wavelength is very close to 805 nm isobestic wavelength and this transmittance variation due to hemoglobin oxygen saturation is negligible. In addition, the optical absorption by ICG is quite high at 810 nm, but quite low at 940 nm. Two LEDs are mounted on one small, glass-epoxy base. The LED base and photodiode are mounted on a flexible printed circuit(FPC).

This FPC is molded by casting polyurethane for electric insulation and mechanical durability. Clinically, as shown in Figure 4.2, the optical sensor is fixed on the tip of the index finger by using a soft adhesive PVC tape to prevent blood congestion and permit this sensor to be attached to a finger tip with any shape.

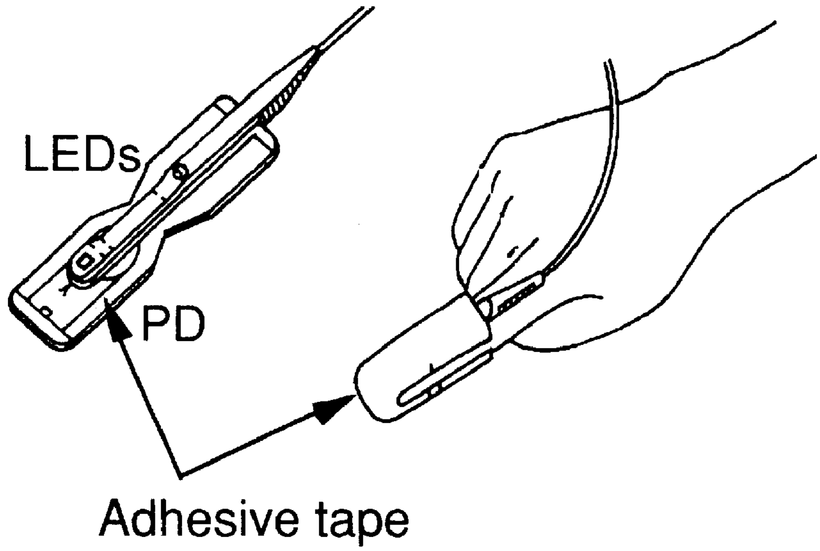

Figure 4.2: Optical Sensor attached to the fingertip
LED; Light Emission Diodes. PD; Photo Diode

4.2.3 The hardware system

Figure 4.3 shows a hardware block diagram. The LEDs are pulsed in order to obtain higher intensity output, to eliminate DC drift problems and to avoid LED overheating. The light transmitted through the finger is detected by the photodiode. The resulting signal from the photodiode is amplified and enters the sample/hold circuits where the difference of the transmittances at each wavelength, and the background are synchronously sampled and held. The sampled DC signal is digitized for computer processing,. then latched in order to be taken into the micro-computer synchronously.

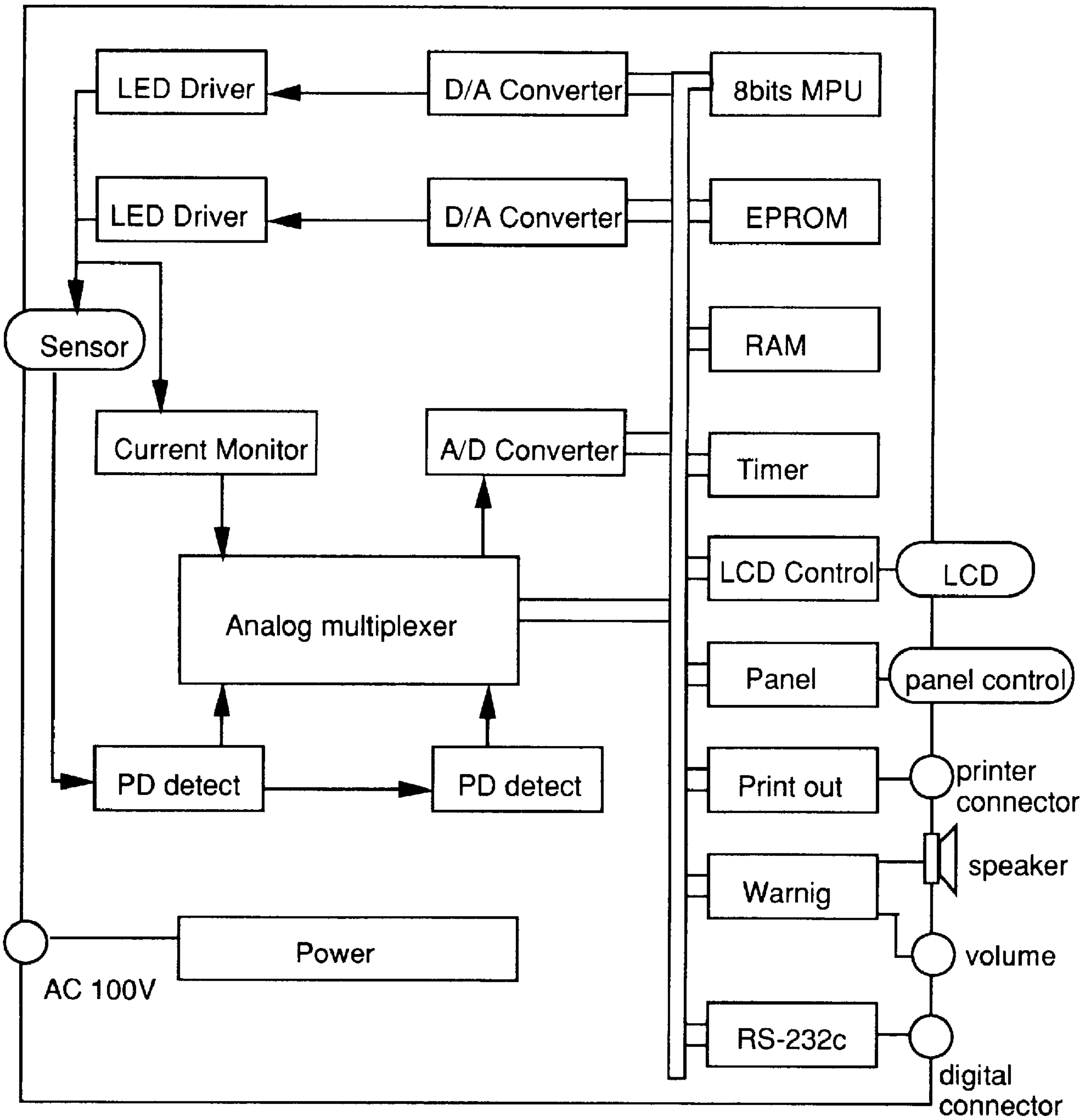

Figure 4. 3 Block diagram of the hardware system

4.3 Results

4.3.1 The system characteristics

This instrument measures the change in the blood ICG concentration over time, and it is necessary that the output of the optical sensor reflect the ICG concentration. Therefore, in order to evaluate the basic performance of this instrument, a standard solution equivalent to the blood ICG concentration during ICG test is prepared. The optical sensor was attached to an optical cuvette filled with the standard solution and sought the relation ship between the ICG concentration and the output voltage, Sg [V], of the sensor. The results, as shown in Figure 4.4, confirmed that the output of the sensor demonstrated a linear relationship with the ICG concentration.

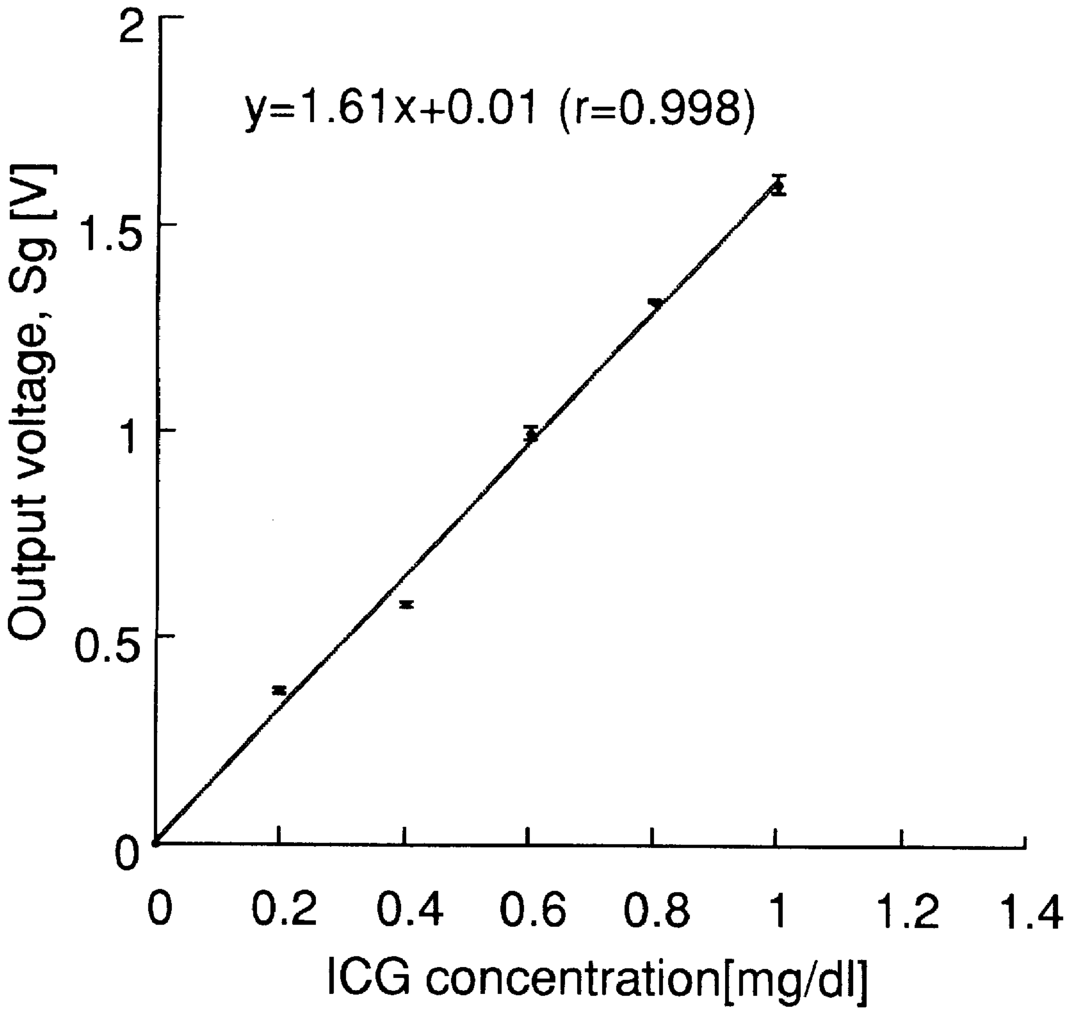

Figure 4.4 The linearity between ICG concentration and output voltage.

4.3.2 Clinical evaluation

4.3.2.1 Method

Hepatic clearance studies were obtained in 16 healthy adult subjects who had histologic evidence of a normal hepatic and 454 patients with biochemical evidence of hepatic diseases (103 chronic hepatitis, 134 liver cirrhosis, 67 hepatoma, 11 acute hepatitis and 139 with other diseases). The optical sensor was attached to the tip of the index finger using adhesive tape. Each patient was injected rapidly without force in the antecubital vein with 0.5mg of ICG per kilogram of body weight.

4.3.2.2 Results

(1) Comparison with blood sampling method

The correlation between values from the blood sampling method and those of the finger-piece method was examined. A correlation equation for K indicated y=0.816x-0.002 (r=0.889) (Figure 4.5). The correlation equation for R_{15} showed y=1.1x+6.4 (r=0.951) (Figure 4.6).

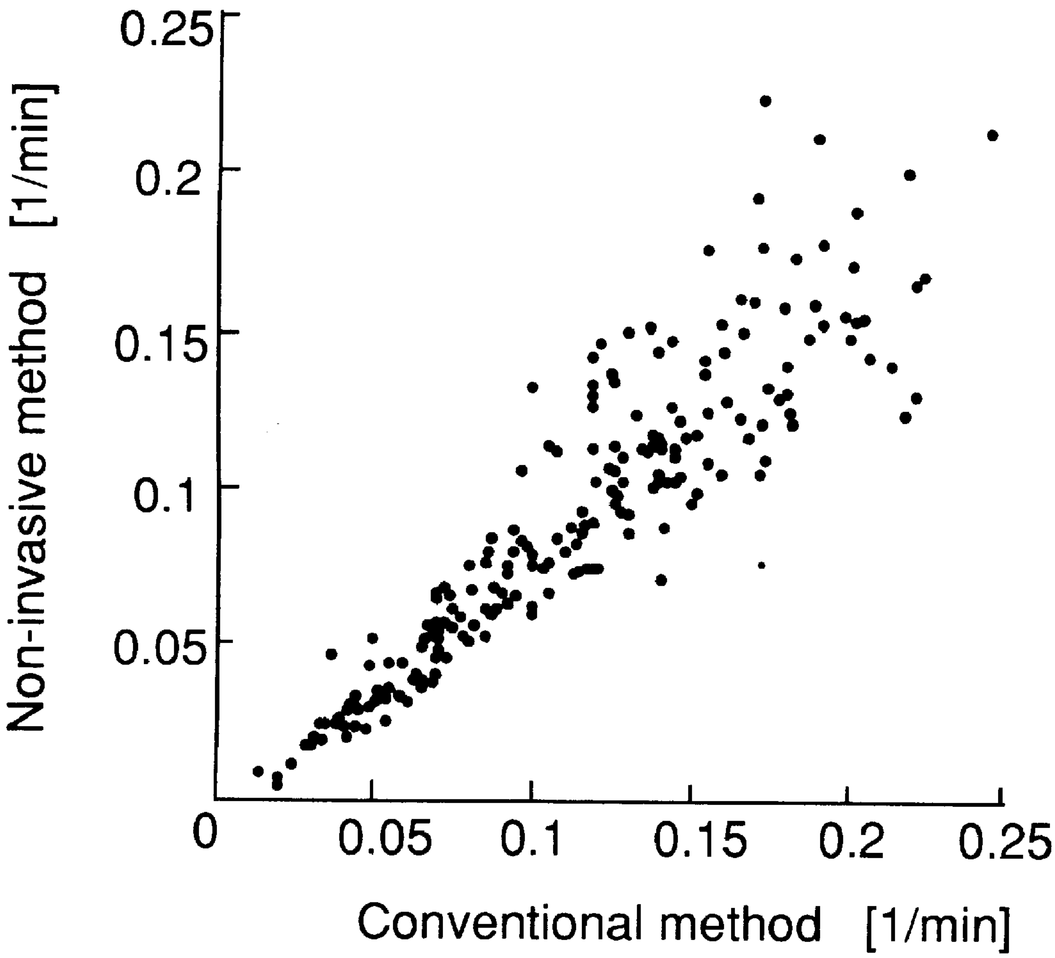

Figure 4.5 K values between conventional blood sampling method and non-invasive method

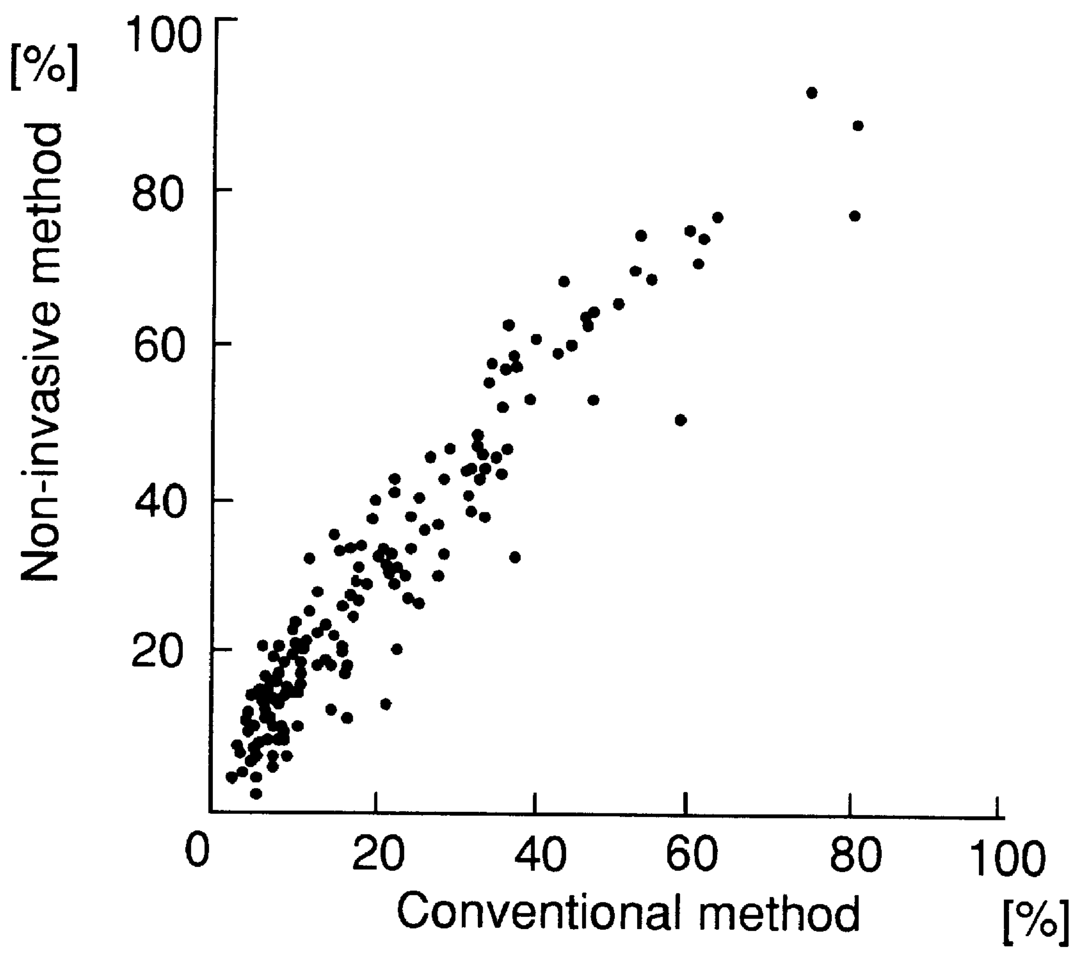

Figure 4.6 R15 values between conventional blood sampling method and non-invasive method.

(2) Values in hepatic diseases

K and R_{15} for various hepatic diseases measured by the finger piece method were examined. Values of K were 0.147 ± 0.022 in the healthy control group, 0.156 ± 0.051 in the acute hepatitis group, 0.118 ± 0.035 in the chronic hepatitis group and 0.071 ± 0.036 in the hepatic cirrhosis group. A significant difference ($p<0.001$) was obtained between the chronic hepatitis group and the control group. Also, there was a significant difference ($p<0.001$) between the liver cirrhosis group and the control group.

Values of R_{15} were 11.63 ± 3.69% in the control group, 13.36 ± 19.16% in the acute hepatitis group, 19.29 ± 8.98% in the chronic hepatitis group and 39.39 ± 19.16% in the liver cirrhosis group. The chronic hepatitis group showed a significant difference ($p<0.001$) from the control group and from the liver cirrhosis group. In addition, the liver cirrhosis group showed a significant difference ($p<0.001$) from the control group. A significant difference was not observed in the liver cirrhosis group between cases with or without primary hepatic carcinoma.

4.6 Discussion

In this Chapter, a description of an instrument for the continuous non-invasive measurement of both K and R_{15} and the results of the clinical evaluation for about 470 patients were presented. The authors propose a biocalibration method before ICG injection particularly *in vivo* measurement, to solve the problem of changing blood volume, satisfactory results were consequently obtained. It is interesting to compare our method with the previous study. For example, Yokosuka et al., settled an idling time to stabilize the change of blood volume. For artifacts, however, this method can be considered as a passive way in comparison with the positive method as explained in this paper. It is not necessary to settle an idling period in the proposed method. Additionally, in the clinical evaluation, the non-blood-sampling method was found to be more convenient because there was no waiting time and no infection, which often results from blood sampling. Another main advantage of this method is that a continuous ICG disappearance curve is obtained. The disappearance curve makes it possible for the progress of hepatic lesions to be diagnosed clearly without calculating K and R_{15}. Moreover, the curve would be helpful for researchers who are interested in the kinetics of ICG, when they construct or analyze compartment models (Paumgartner 1970, Ishigami 1988, Kanda 1988) based on the compartment analysis.

4.7 Conclusion

In this chapter, the we discussed the method of testing the hepatic clearance of a dye and its clinical application. A high correlation between the values obtained by this method and by the blood sampling method was observed, showing that the ICG test by the finger-piece method is considered to be a useful and sensitive method for clinical use. Furthermore, this method might be useful for testing the liver before and after liver transplantation.

CHAPTER 5

NUMERICAL ANALYSES FOR ICG CLEARNACE IN A TURBID MEDIA

5.1 Introduction

Indocyanine green (ICG) (Fox 1957) described in the previous chapter is a tricarbocyanine dye that has been used for measuring cardiac output and hepatic function in human for 30 years. Especially in Japan, it has been widely used as a sensitive tracer in hepatic dye clearance tests (Namihisa 1963). However, Several blood samplings are required to determine the plasma disappearance rate (k) of ICG by using a spectrophotometer. In Chapter 4, as an ICG test without blood sampling, the finger piece method using an optical sensor was described (Awazu 1990, Namihisa 1990).

Briefly, the finger piece method was carried out as follows; an optical sensor consisting of two LEDs and a photodiode is fixed to the tip of the finger, calibration is conducted by raising and lowering the arm to compensate the changing of the blood volume at the measuring site, then ICG is administered intravenously and the optical sensor measures the optical transmittance through the finger to calculate k . Clinical results showed in Chapter 4 tells us good relationship between the non-invasive method and the conventional blood sampling method. It is cliniccaly useful, however, the calculation to determine the plasma disappearance rate, k in 1/min, is based on the transmittance of light through the fingertip, but tissues such as the finger tip should be considered as highly optically scattering matters.

In such a light-tissue interaction, it is important to model light transport in tissues, which are turbid media. Among the available models are Monte Carlo simulations,(Pickering 1993, Firbank 1993, Wilson 1990, Jacques 1993, Patterson 1989, Jacques 1994, Liu 1993) diffusion theories, (Patterson 1991, Tromberg 1993, Thomsen 1994, Hielscher 1994, Farrell 1992, Kienle 1994, Farrell 1992) and finite difference methods,(Groenhuis 1983). As a mathematical model to treat turbid tissues, Monte Carlo simulations of photon propagation offer a flexible yet rigious approach toward photon transport (Wang 1992). But, it takes a long time to get the result using Monte Calro simulation. On the other hand, diffusion approximation has a possibility to give an adequate solution for the same problem in a short time. Therefore, in this Chapter, the both methods are applied to the light propagation in a slab model to simulate the actual transpotation pf the light through the fingertip as a simple slab. The simulation results are compared with *in vivo* result to examine the effectiveness of scattering to the plasma disappearance rate.

5.2 Materials and methods

5.2.1 Monte Carlo simulation

The Monte Carlo method is a method to estimate the exact solution to light distributions. This is done by the set of all possible paths of photons through objects. To compute the light distributions according to tissue geometries and optical properties, including refractive index (n), absorption coefficient (μ_a), scattering coefficient (μ_s), and anisotropy factor (g), Monte Carlo program is written for turbid media such as tissues. The delta- scattering technique was used for photon tracing to greatly simplify the algorithm because this technique allows a photon packet to be traced without worrying about the interfaces between tissues. This technique can be used only for refractive-index-matched tissues, although it allows the ambient clear media (e.g., air) and the tissue to have mismatched refractive indices. The tissue system is assumed to have multiple tissue types with matched refractive indices. The interaction coefficient of the ith tissue type, defined as the sum of μ_a and μ_s, is denoted by, μ_i. The techniques is briefly summarized as follows.

1. Define a majorant interaction coefficient μ_m, $\mu_m \geq \mu i$, μi for all i.
2. Select a distance R,

$$R = - \ln(x) / \mu_m, \tag{5.1}$$

where x is a uniformly distributed random number between 0 and 1 ($0 < x < 1$). Then, determine the tentative next collision site **rk**' by:

$$\mathbf{r}k' = \mathbf{r}k\text{-}1 + R\mathbf{u}k\text{-}1, \tag{5.2}$$

where **r**k-l is the current site and **u**k-l is the direction of the flight.

3. Play a rejection game:

a. With a probability of $\mu(\mathbf{r}k')/\mu_m$, accept this point as a real interaction site (**r**k =**r**k');

b. Otherwise, do not accept **r**k' as a real interaction site but select a new path starting from **r**k' with the unchanged direction **u**k-l (i.e., set **r**k-l = **r**k' and return to Step 2).

An imaginary interaction event that changes neither the weight nor the direction of the photon is introduced to understand the validity of this algorithm. This definition implies that such imaginary interactions are not physically observable, i.e., they can be introduced with any interaction coefficient at any point. Now if the majorant interaction coefficient (μ_m) is a sum of the real (μ_{re}) and imaginary (μ_{im}) interaction coefficients, then in the procedure outlined above, a fraction of the interactions,

$$1 - \frac{\mu_{re}}{\mu_m} = \frac{\mu_{im}}{\mu_m} \tag{5.3}$$

are imaginary interactions. On ten average, for every μ_m total interactions, there will be μ_{re} interactions accepted as real interactions. The mean free path for the majorant interactions in the delta-scattering method is $1/\mu_m$ and the mean free path for the real interactions in the direct method is $1/\mu_{re}$. Therefore, the photon will move to the correct interaction site using the delta-scattering technique as it would using the direct method, i.e.,

$$\mu_m(1/\mu_m) = \mu_{re}(1/\mu_{re}) \tag{5.4}$$

where the left-hand side is the average distance traveled by the photon packet with μ_m total steps or with μ_{re} real interactions in the delta-scattering method and the right-hand side is the average distance traveled with μre real interactions in the direct method. During the tracing of each weighted photon, the light absorption, reflectance, or transmittance are correspondingly scored into different arrays according to the spatial and temporal positions of the photon. Multiple photons are traced to achieve an acceptable statistical variation.

5.2.2 Diffusion theory

When using photon diffusion theory, the optical properties needed are the absorption coefficient (μ_a) and reduced scattering coefficient ($\mu_s'=(1-g)\mu_s$). Two related coefficients are the transport interaction coefficient(μ_t') and the effective attenuation coefficient (μ_{eff}), which are respectively expressed by the following relationship:

$$\mu_t' = \mu_a + \mu_s' \tag{5.5}$$

and

$$\mu_{eff} = \sqrt{3\, \mu_a\, \mu_t'} \tag{5.6}$$

The inverse of the transport interaction coefficient is defined as one transport mean path (mph' = $1/\mu_t'$)

Diffusion theories for semi-infinite tissues have been presented elsewhere (Farrell 1992). Here, The diffusion theory is extended for tissue slabs such as the fingertip. An infinitely narrow laser beam (pencil beam) is incident upon a tissue slab whose optical properties are refractive index n s', and thickness d. The pencil beam is approximated by an isotropic point source that is 1 mfp' below the tissue surface. A cylindrical coordinate system is set up, where the z axis originates on the top tissue surface and points downward perpendicularly to the tissue surface. The steady state diffusion equation for a homogeneous medium is:

$$S - \mu_a = -\Delta\nabla^2 \phi \tag{5.7}$$

In this cylindrical coordinate system, the fluence caused by an isotropic point source at $z = z_s$ in an otherwise infinite medium has been analytically solved. The response to a point source S is:

$$\phi(z,r,z_s) = \frac{1}{4\pi D}\frac{\exp(-\mu_{eff}\rho)}{\rho} \tag{5.8}$$

where z and r are the cylindrical coordinates of the observation point and p is the distance between the observation point and the source, i.e.,

$$\rho = \sqrt{(z-z_s)^2 + r^2} \tag{5.9}$$

and D is the diffusion constant,

$$D = \frac{1}{3\mu_t'} \tag{5.10}$$

Since we are interested in the transmittance on the bottom tissue surface, the contribution of this isotropic point source is

$$J(z=1,r,z_s) = D\frac{\partial\phi}{\partial z}\bigg|_{z=1} = -\frac{(1-z_s)(1+\rho)\exp(-\mu_{eff}\rho)}{4\pi\rho^3} \tag{5.11}$$

To compute the fluence caused by an isotropic point source in a tissue slab based on Eq.(5.8) We need to convert the slab into an infinite medium by satisfying the boundary condition with an array of image sources. Since the fluence on the two real boundaries is not zero, two extrapolated virtual boundaries where the fluence is approximately zero are used. The two virtual boundaries are the distance Zb away from the tissue surfaces, where Zb is

$$Zb = 2\ A\ D, \tag{5.12}$$

where A is related to the internal reflection ri. When the boundary has matched refractive indices, A = 1; otherwise, A can be estimated by

$$A = \frac{1 + r_i}{1 - r_i} \tag{5.13}$$

$$r_i = -1.440\ n_{nel}^{2} + 0.710\ n_{nel}^{-1} + 0.668 + 0.0636\ n_{nel} \tag{5.14}$$

where n_{nel} is the relative refractive index of the tissue (Groenhuis 1983). Figure 5.1 shows the positions of the original isotropic point source and its image sources about the two virtual boundaries. Each mirroring changes the sign of the point source. The z coordinate of ith positive or negative image source is

$$Zi(\pm) = -Zb + i\ (d + 2Zb) + (z_o + Zb). \tag{5.15}$$

Once theses image sources are used, the boundary condition is approximately satisfied, and hence the true boundaries can be removed. The problem is converted into an array of isotropic sources of both signs in an infinite medium. A linear combination of Eq. (5.8) for different source positions will, therefore, yield the fluence of the isotropic point source in the original tissue slab, and a linear combination of Eq.(5.11) for different source positions will yield the transmittance.

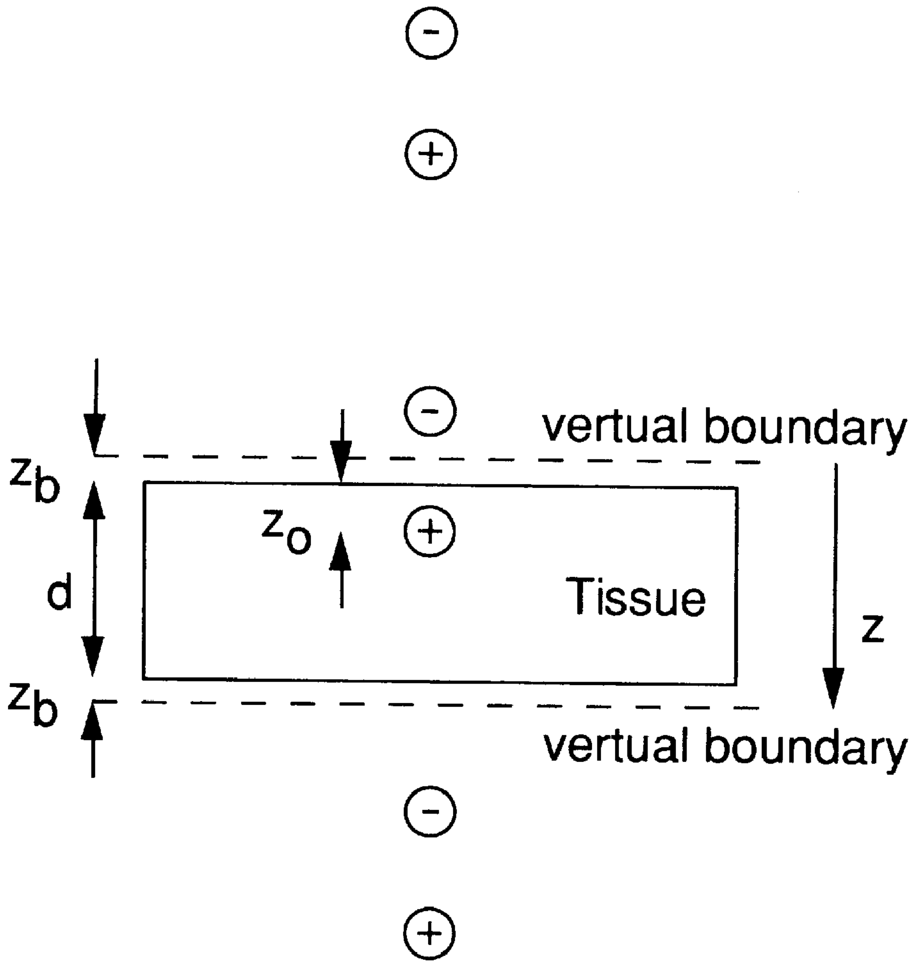

Figure 5.1: Distribution of the image source for a tissue slab. The original isotropic point source is z=1 mfp' below the tissue surface

5.2.3 Optical model for the finger tip

A tissue optical such as the fingertip is first considered as an optically homogeneous. Incident light comes in from the upper layer of the tissue model, and a detector detects transmitted light from the bottom layer of the tissue model. Optical properties such as tissue and blood at the wavelength with the maximum ICG absorption, 805 nm, are determined using published data (Landsman 1978). ICG optical property at various concentrations at 805nm is measured in 0.5% - albumin solution using a spectrophotometer.

5.3 Results

5.3.1 ICG optical property using a spectrophotometer

Figure 5.2 shows the ICG concentration in 0.5%-albumin solution versus absorption coefficient μ_{aig} [cm^{-1}] using a spectrophotometer. The linear relationship can be found between the ICG concentration and μ_{ai}. From the equation fitted, μ_{ai} in [cm^{-1}] is

$$\mu_{ai} = 2.58\ C_{ig} \qquad (5.16)$$

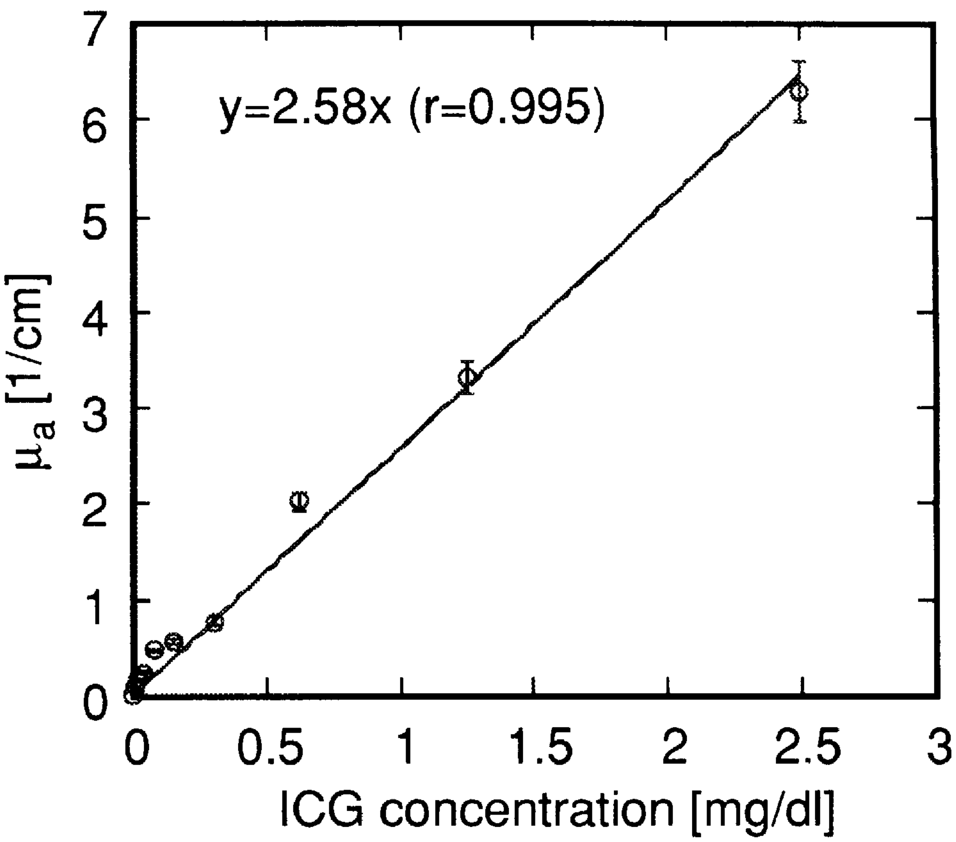

Figure 5.2: ICG concentration versus absorption coefficient in a clear media

where Cig is ICG concentration in 0.5% albumin solution. Since low percentage albumin solution can be considered as a non scattering matter, spectrophotometric analysis is not affected by scattering in this range.

5.3.2 Simulation results of Monte Calro method and diffusion approximation.

First, a typical set of tissue optical with refractive index between air and tissue $n_{rel}=1.37$, $g = 0.95$, $\mu_t = 0.478 + \mu_{ai}\ cm^{-1}$, $\mu_s=545.2\ cm^{-1}$ and $\mu_s' =27.3\ cm^{-1}$ is assigned to the model. Second, the background absorption or scattering are varied to estimate their effect to the decay constant.

In Figure 5.3, the results of the method computing the diffuse transmittance based on the diffusion theory is compared with those computed by the Monte Carlo method (Wang 1992), in which the Monte Carlo simulation results are considered accurate. Although the number of image sources is infinite, the series is truncated after four pairs of sources. For the diffuse transmittance, the diffusion theory seems to be accurate, but the Monte Carlo simulation result is too noisy to permit a definitive conclusion especially at low ICG concentration because of statistical errors. The other disadvantage of the Monte Carlo method is that programs have to run for a long time

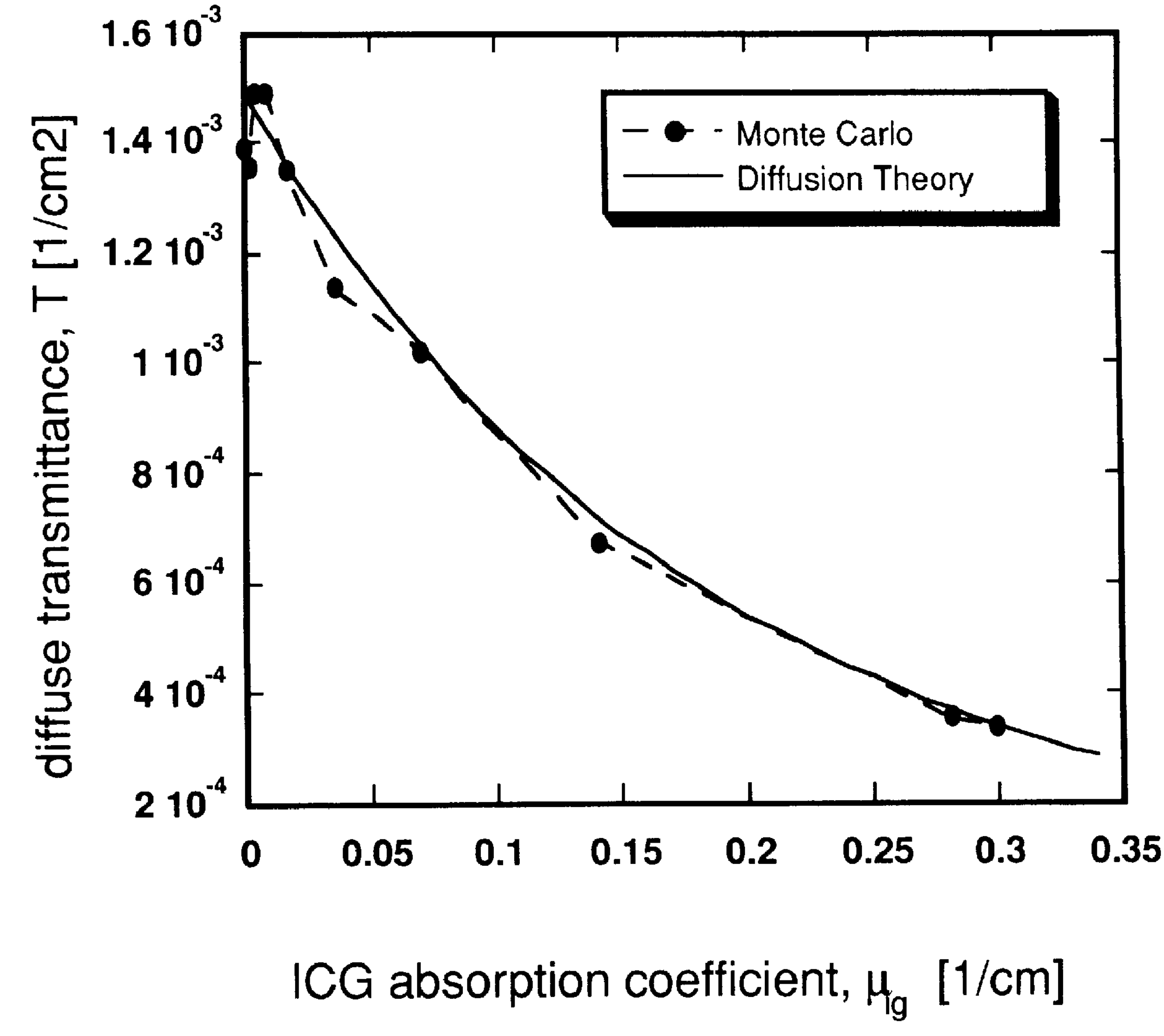

Figure 5.3 Diffuse transmittance of a pencil beam incident upon a tissue slab are computed with the diffusion theory and compared with the Monte Carlo simulation The slab thickness is 1 cm, nd the optical properties of the tissue are refractive index $n_{rel}=1.37$, $\mu_{abm}=0.478$ cm^{-1}, and $\mu_s'=27.3$ cm^{-1}

to give accurate estimates. Following the low of large numbers, the average values are estimated without bias, but the standard deviation of the estimated average values only decreases as $1/\sqrt{N}$, where N is the number of photons generated. In this case 1,000,000 photons were used to calculate, and the calculation time was about 24 hours by Sun workstation. Therefore, diffusion approximation can give an appropriate result to examine the dependence of scattering in this model with a simple geometry such as a slab model.

Figure 5.4 shows the diffuse transmittance, T, of a tissue model with ICG having different background absorption coefficient . According to these simulation results, when the tissue has high absorption such as 1.2 [cm^{-1}] or more, the relationship between the ICG absorption coefficient determined by the concentration and the diffuse transmittance is linear, but a tissue with low background 0.8 [cm^{-1}] or less has not linear relationship.

In actual transmittance measurement used a photodetector, the measuring values are equal to -ln(T) which can be called an apparent absorption coefficient, $\mu_{a(app)}$ because the pathlength of the model is 1 cm. Figure 5.5 shows the relationship between calculated $\mu_{a(app)}$ by the diffusion approximation and ICG absorption coefficient. This also implies the non-linearity between ICG concentration and measured value because of the scattering and background effect.

5.3.3 Estimation of the decay constant of ICG using the diffusion approximation

Using the above simulation results based on the diffusion theory, the decay constant, so called plasma disappearance rate, k in min^{-1}, is examined for various conditions. The k is defined as

$$C_{ig} = C_o \exp(-k \cdot t) \tag{5.17}$$

where C_o in mg/dl is initial ICG concentration, and t in minuets is time after ICG was injected intravenously. Usually, Cig is measured as ICG concentration in blood plasma using spectrophotometer. Samples included ICG are treated as non-scattering media because there are no tissues and blood cells. Therefore, there is a linear relationship between μ_{ai} and C_{ig} descried in section 5.6.1. In a turbid media such as a tissue, however, there is no linear relationship between $\mu_{a(app)}$ and Cig determined by the absorption coefficient of ICG, μ_{ai}, described in section 5.6.2.

Figure 5.6 shows typical ICG clearance curves estimated using k values determined by a spectrophotometer and the diffusion theory. It is clear that the curves in a clear media are different from those

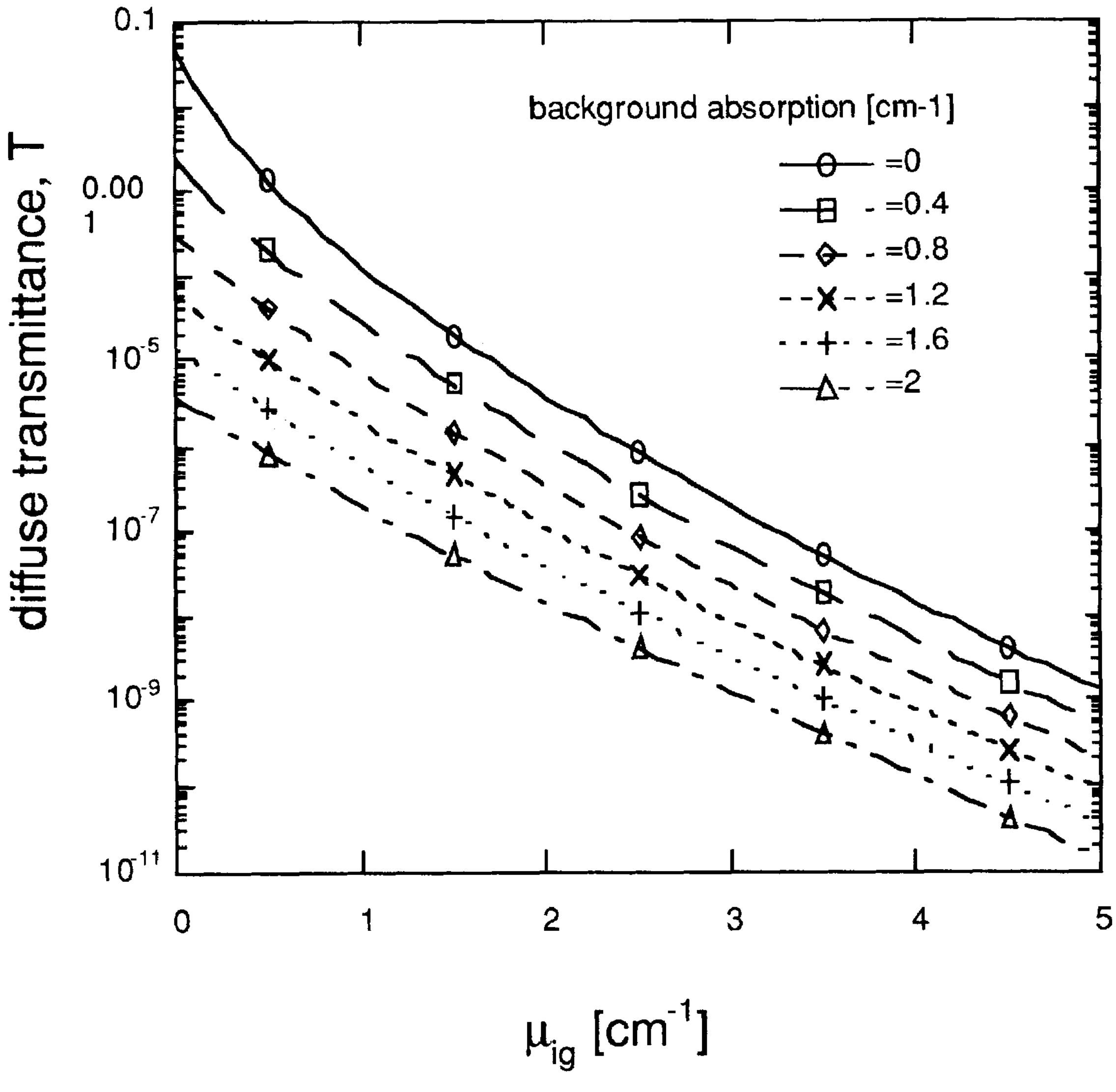

Figure 5.4: Diffuse transmittance with various background absorptions and scattering

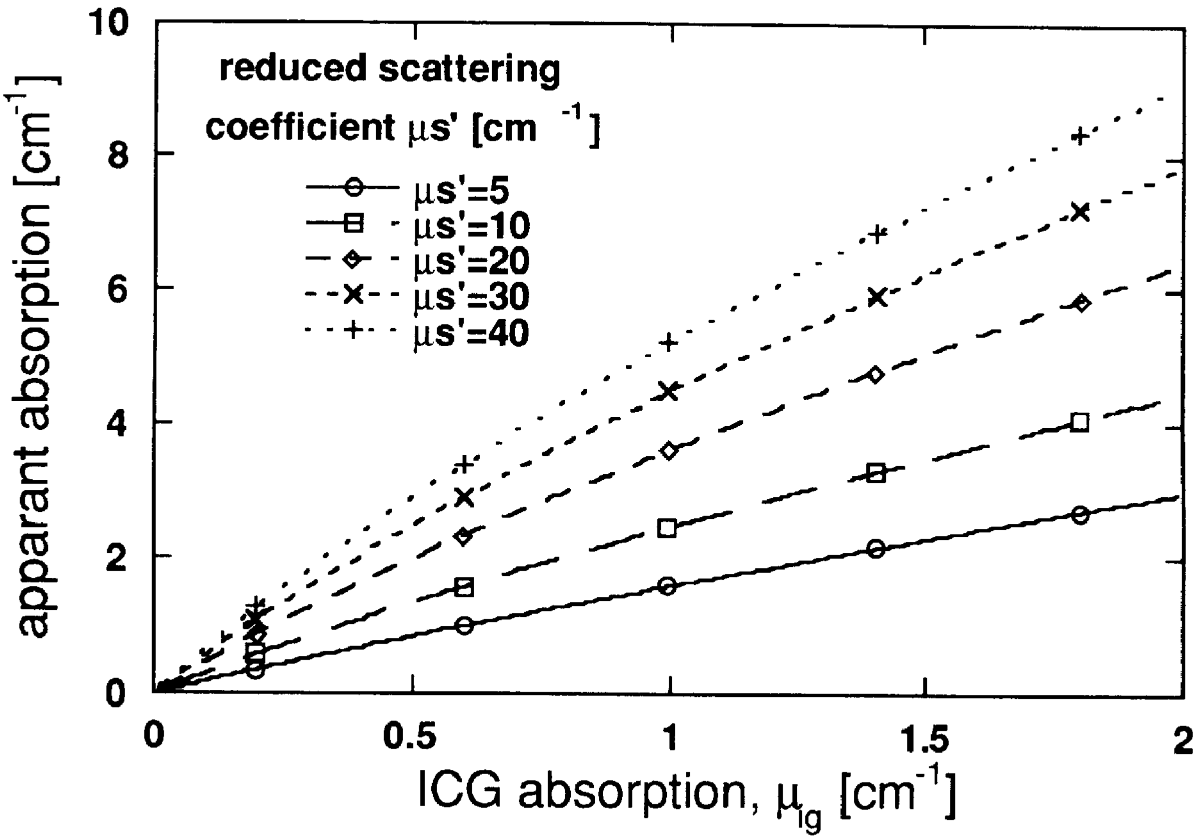

Figure 5.5 relationship between calculated $\mu_{a(app)}$ by diffusion approximation versus ICG absorption coefficient for various background absorption and scattering

curves measured by the diffuse transmittance through the model proposed. This implies calculated k in a clear media, k_c, is different from k in a turbid media, k_t. Expanding these results. Figure 5.7 shows the relationship between k_c and k_t. Clinically, the linear regression equation between k_c and k_t is known as $k_t=0.816k_c$ (Namihisa 1990). Therefore, the diffusion approximation also gives a well fitted results compared to the clinical data.

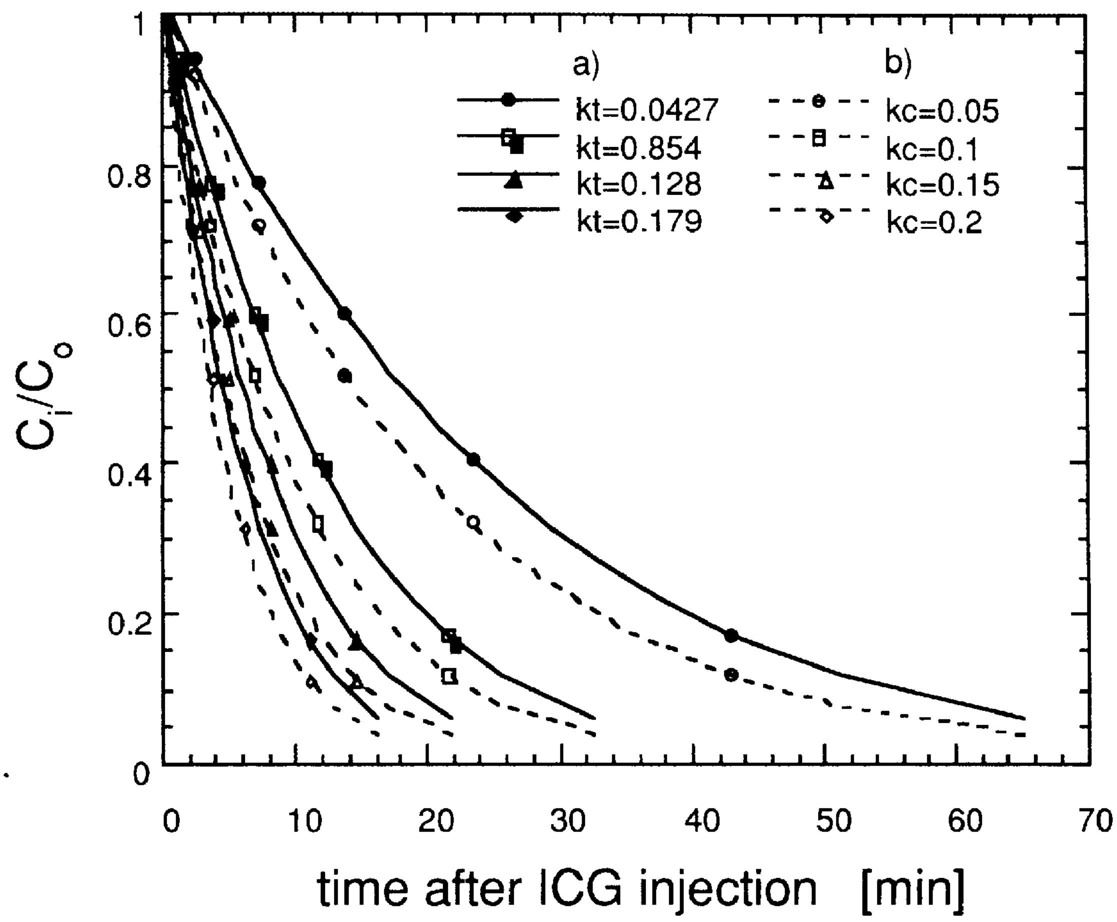

Figure 5.6: a) Clearance curves considered turbidity. b) Typical ICG clearance curve calculated using k_c values determined by a spectrophotometer.

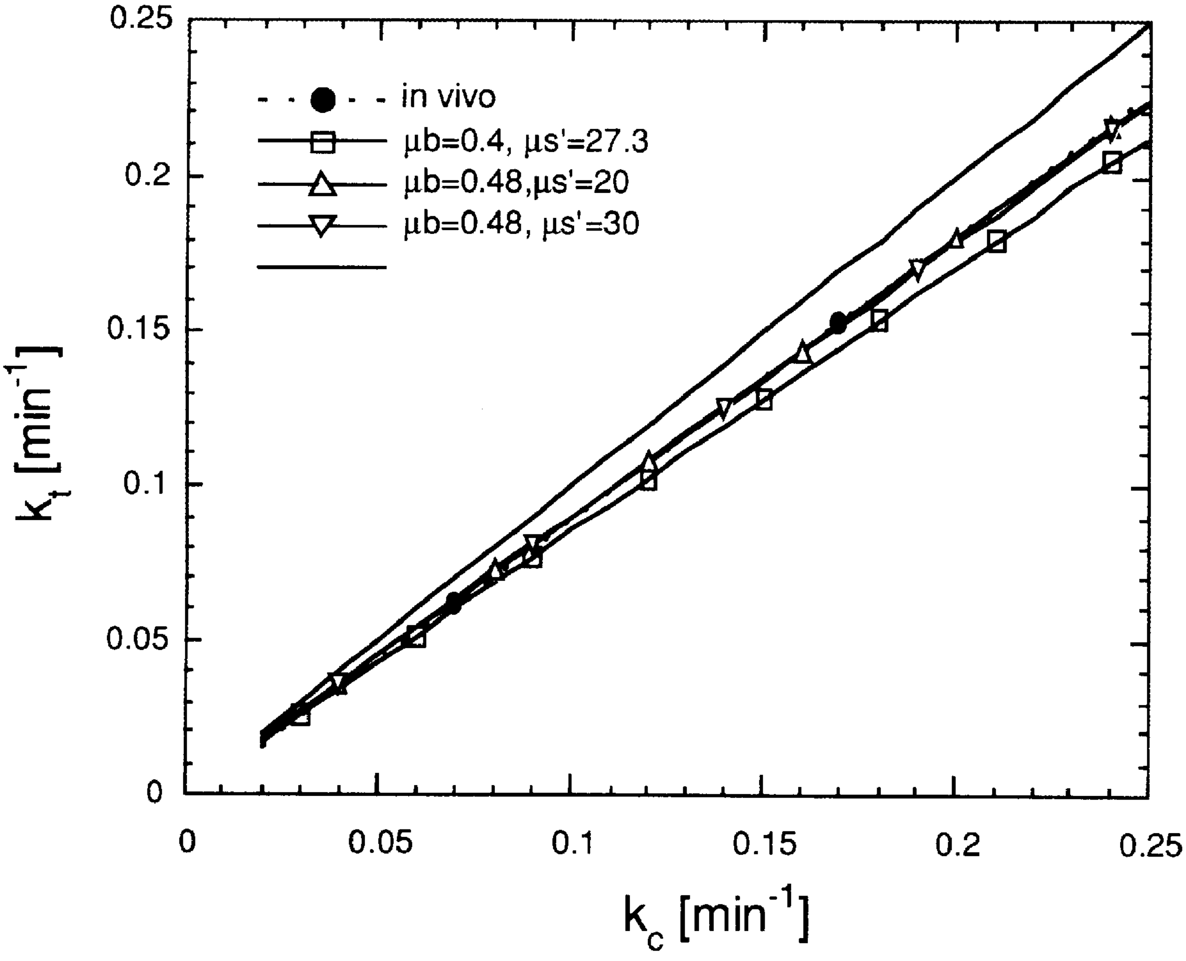

Figure 5.7 Estimation of k_t by the ICG clearance curve using known amount of k_c value.

5.4 Discussion

To measure the decay constant of a dye concentration such as ICG directly from measuring site *in vivo*, knowing optical properties such as absorption and scattering coefficient is important because the scattering and background absorption produce lower number of decay constants called plasma disappearance rate. The summation of clinical data may solve this problem, but theoretical analysis is still powerful to analyze the effect. In actual *in vivo* measurements, various thickness and tissue optical properties should be considered.

5.5 Conclusion

An optical tissue model for ICG test is proposed to simulate the light propagation in the finger tip using the Monte Carlo method and diffusion theory. The diffuse transmittance based on the diffusion theory gave more stable results than that based on the Monte Calro simulation for this model. The simulation results show that scattering and back ground absorption produce the smaller value of the decay constants than the values measured using a spectrophotometer. Clinical data was well fit the simulation result.

CHAPTER 6

CONCLUSION

In this thesis, kineticis of dye in tissue and cells are measured by optical methods. The modeling of compartment system that can deal with the kinetics of the dyes is proposed in chapter 2, and lasers or light emission diodes are used for measuring fluorescence or transmittance of the target dyes. Using these methods, the compartmental analysis with experimental results of the fluorescence and the transmittance taken from collagen-membrane, rat-cancer-cells, or human-tissues gives the kinetics of the dyes. This results are discussed the viability of the rat-cancer-cells in chapter 3 or human-liver-function in chapter 4. For the tissues considered optically scattering, mathematical simulation methods are proposed to evaluate the dependence of the scattering for the disappearance rates of the dye in chapter 5. These chapters are summarized as follows.

1) In Chapter 2, The fixation of a photosensitive reagent, tetrabrominated rhodamine (TBR), onto collagen gels was studied as a model for photolabeling biological tissues with medical reagents. The kinetics of photolabeling process was modeled using a compartmental model. Parameters of the model were determined by experiments on tissue simulated gel films. The results showed that photolabeling is a powerful way to measure the optical propagation

in tissue and also the compartmental analysis tells us the quantitative information about the photo-chemical processes. The results also suggested that DMSO has replaced some of the water around collagen thereby disrupting the water structure and permitting TBR to move closer to the collagen for more efficient bonding upon photoactivation by debromination.

2) Chapter 3 was concerned with photo-dynamic therapy (PDT) using PPIX for single cancer cell. The amount of PPIX attained by the cells ranged between 1-15 μg/g cells, with a mean value of 6.0 μg/g cells. The photobleaching dose constant was 135 ± 56 J/cm^2. The photodynamic dose obtainable after complete photobleaching ranged between 2e18-5e19 with a mean value of 5.2e19 [photons absorbed by PPIX per g cells]. A colony formation study indicated that the threshold D_{PDT} required for cell killing fell in the range of 1e18-3e19. Therefore, to make a suitable protocol for PDT, the threshold of D_{PDT} for single cell is much more important than the average value of D_{PDT}. Furthermore, calibration methods developed in this chapter give advantages for determine the absolute concentration using fluorescence.

3) In Chapter 4, a non-invasive method for an ICG test of hepatic function was developed. A high correlation between the values obtained by this method and by the blood sampling method was observed, showing that the ICG test by the finger-piece method is considered to be a useful and sensitive method for clinical use.

4) In chapter 5, an optical tissue model for ICG test is proposed to simulate the light propagation in the finger tip using the Monte Carlo method and diffusion theory. The diffuse transmittance based on the diffusion theory gave more stable results than that based on the Monte Calro simulation for this model. The simulation results show that scattering and back ground absorption produce the smaller value of the decay constants than the values measured using a spectrophotometer. Clinical data was well fit the simulation result.

As we mentioned, we have dealt with 3 types of materials using kinetic analysis of the dyes in tissues and cells. The study of light-tissue interaction offers the opportunity to optimize clinical or experimental protocols. Especially, the variety of monochromatic light such as lasers available to medicine continues grow, and more sophisticated protocols are under development. Industry has found that optical systems designed for medicine can be commercial successes (e.g., ophthalmology and dermatology), and its interest in the medical optics market is increasing. The study of mechanisms of light -tissue interaction can guide the industry related to electro-optics in its development of new devices for medical applications.

REFERENCES

Ades I.Z. (1990)."Heme production in animal tissues:The regulation of biogenesis of d-aminolevulenate synthetase," *Int. J. Biochem.* Vol. 22, pp. 565-578.

Aoyagi, T. and K.Yamaguchi (1975)."Ear piece method for measuring cardiac output,"*Proc. 14nd conf. JJME* 2-A-1.

Arnon, S. and N.S. Kopeika (1994)."Effects of particulates on performance of optical communication in space and an adaptive method to minimize such effects," *Appl. Opt.*, Vol. 33, pp. 4930-4937.

Athar, M., H. Mukhtar and D. R. Bickers (1988). "Differential role of reactive oxygen intermediates in photofrin-I and photofrin-II-mediated photoenhancement of lipid peroxidation in epidermal microsomal membranes," *J. Invest. Dermatol.*, Vol. 90, pp. 652-657.

Awazu K., Watanabe S., Namihisa T. (1990). "Clinical evaluation of indocyanine green using the optical finger piece method," *Asian Pacific Study of the Liver.*

Awazu K., Watanabe S., Namihisa T. (1990). "Multicenter study of indocyanine green tests by non-invasive optical finger-piece method," *International Association of the study of the Liver.*

Awazu K., Matsubara H., Niwa S., etal (1992). "The development of ICG clearance meter RK-1000," *Sumitomo Electric Technical Review*, No.34, pp96-100.

Awazu K., Jacques S.L. (1995). "Quantitative fluorescence microscopy yields distributions of concentration and photo bleaching rate in 5ALA-induced protoporphyrin IX in cell population," *SPIE* 2392, pp77-84.

Awazu, K., S. Watanabe , A. Miyazaki , T. Namihisa (1990)."ICG Disappearance in patients with various liver diseases analyzed using finger-piece method," *Mathematical modeling of Liver excretory Processes*, pp.92-101.

Bedwell J., A.J. MacRobert, et al. (1993). "Fluorescence distribution and photodynamic effect of ALA-induced PPIX in the DMH rat colonic tumor model," *Br. J. Cancer* Vol. 65 pp. 818-824.

Chance, B., H. Leigh, H. Miyake, D. Smith and S. Nioka (1988). "Comparison of time resolved and un-resolved measurements of deoxyhemoglobin in brain," *Proc. Natil. Acd. Sci., Vol. 85, pp4971-4975.*

Chen Q., S. Shetty, L. Heads, D. Schultz, J. Cemy, H. Chen, F.W. Hetzel (1994)."Photodynamic therapy of normal canine prostate," Abstract 167, *5th International Photodynamic Association Biennial Meeting*, Amelia Island, FL, Sept. 21-24.

Cherrick, G., S. Stein, C. Leevy and C. Davidson (1960). "Indocyanine green: Observation on its physical properties plasma decay and hepatic extraction," *J. Clin. Invest.*, Vol. 39, pp. 592-600.

Cheung, P. W. (1973). "Effects of blood physiological variations on optical scattering and fiberoptic oximetry," PhD. Dissertation, University of Washington, Seattle, WA.

Delpy, D.T., M. Cope, S. Arridge, S. Wray and J. Wyatt (1988). "Estimation of optical path length," *Phys. Med. Biol.*, Vol. 33, pp. 1433-1442.

Dimitrios X. G. D., K.C. Kennedy, et al. (1990)."Phototoxic damage to sebaceous glands and hair follicles of mice after systemic administration of 5-aminolevulinic acid correlates with localized protoporphyrin IX fluorescence,"*Amer. J. Pathology* Vol. 136, pp.891-897.

Ezekiel S. (1982). *Fiber-Optic Rotaion Sensors*, Springer-Verlag, Berlin.

Farrell, T. J. , B. C. Wilson, and M. S. Patterson (1992). "The use of a neural net vork to determine tissue optical properties from spatially resolved diffuse reflectance measurements," *Phys. Med. Biol.,* Vol. 37, pp. 2281-2286.

Farrell, T. J. , M. S. Patterson, and B. C. Wilson (1992)."A diffusion theory model of spatially resolved, steady-state diffuse reflectance for the non-invasive determination of tissue optical properties *in vivo,*" *Med. Phys.*, Vol. 19, pp. 879-888.

Firbank, M. , M. Hiraoka, M. Essenpreis, and D. T. Delpy (1993). "Measurement of the optical properties of the skull in the wavelength range 650-950 nm," *Phys. Med. Biol.,* Vol. 38, pp.503-510.

Flock, S.T., B. C. Wilson and M. S. Patterson (1989). "Hybrid Monte Carlo diffusion theory modeling of light distribution in tissue," *SPIE* Vol. 908, pp. 20-28.

Fox, I.J., L.G.S.Brooker, D.W. Heseltine, et al. (1957). "A tricarbocyanine dye for continuous recording of dilution curves in whole blood independent of variations in blood oxygen saturation,"*Fed. Proc.,* Vol. 16, pp. 39

Galliorenzi, T.J. and J.A. Bucaro (1982)."Optical fiber sensor technology," *IEEE J.Quantum Electron.,* Vol. QE-18, pp. 626-665

Gomer, C. J., N. Rucker, A. Ferrario and S. Wong (1989). "Properties and applications of photodynamic therapy," *Radiat. Res.*, Vol. 120, pp. 1-18.

Groenhuis, R. A. J., H. A. Ferwerda, and J. J. Ten Bosch (1983)."Scattering and absorption of turbid materials determined from refection measurements.I:Theory," *Applied Optics*, Vol. 22, pp. 2456-2462.

Hahne, A. and R. Furch (1987)."Optical space communications: ESA activities and plans," *Optical Technologies for space Communication Systems*, Vol. 745, pp. 2-8.

Hampton, J.A., and S. H. selman (1992). "Mechanism of cell killing in photodynamic therapy using a novel *in vivo* drug/ *in vitro* light culture system," *Photochem. Photobiol.* Vol. 56, pp. 235-243.

Hasan, T., C.R., Shea, (1989). "Rhodamine dyes as potential agents for photochemotherapy of cancer in human bladder carcinoma cells," *Cancer Research* Vol. 49, pp. 3961-3965.

Hasegawa, A. and Y. Kodama (1981)."Signal transmission by optical solitons in monomode fiber," *Proc. IEEE*, Vol. 69, pp. 1145-1150,

He X-Y, S. L. Jacques, S. L. Thomsen (1994)."In vitro cellular effects of δ-aminolevulenic acid sensitized photo-dynamic therapy," *SPIE* Vol. 2133, pp. 18-27.

Hecht, E. (1990). *Optics:Twentieth-Century Optics*, Addison-Wesley Publishing, pp. 8-11

Henderson, B. W., S. M. Waldow and T. S. Mang (1985). "Tumor destruction and kinetics of tumor cell death in two experimental mouse tumors following photodynamic therapy," *Cnacer Res.*, Vol. 45, pp. 572-576.

Hielscher, A. H. , H. Liu, F. K. Tittel, B. Chance, L.-H. Wang, S. L. Jacques (1994)."Determination of blood oxygenation in the brain by time-resolved reflectance spectroscopy I," *SPIE*, Vol. 2136A, in press.

Howard, M.M. and C.M.Leevy (1967)."Indocyanine Green Clearance as a Test for Hepatic Function," *JMMA,* Vol. 200, pp.148-152.

Ishigami, Y. (1988)."Constant Measurement of indocyanine Green(ICG) Removal using a Finger-piece Optical Sensor and Its Clinical Application for Patients of Diseased Hepatic," *Jpn. Pharmacol. Ther.* Vol. 16, Suppl.1, pp.47-54.

Jacques, S. L. and S.T. Flock (1991). "Time-resolved reflectance spectroscopy," *SPIE proceedings* Vol. 1525, pp. 35-40.

Jacques, S. L., and S. A. Prahl (1987). "Modeling optical and thermal distribution in tissue during laser irradiation," *Laser Surg. Med.,* Vol. 6, pp. 494-503.

Jacques, S.L. (1991). "Principle of phase-resolved optical measurements," *SPIE Proceedings*, Vol. 1525, pp. 143-153.

Jacques, S.L., T. Hasan (1992). "Mapping radiant energy distribution during laser irradiation of collagen phantoms by photolabeling with tetrabrominated rhodamine," *Proc. Soc. Photo-opt. Instr. Eng., Laser-Tissue Interaction III,* Vol. 1646, pp. 219-226.

Jacques, S. L. , A., Gutsche, J. A. Schwartz, L. H. Wang, and F. K. Tittel (1993)."Video reflectometry to extract optical properties of tissue in vivo," *SPIE*, Vol. 11, pp. 211-226 .

Jacques, S. L. , L.-H. Wang, A. H. Hielscher (1994)."Time-resolved photon propagation in tissues," In: A. J. Welch, M. J. C. van Gemert (ed.), *Optical Thermal Response of Laser Irradiated Tissue, in press*; Plenum Publishing Corp., New York.

Jacques, S. L., A. Gutsche, J. A. Schwartz, L. -H. Wang and Frank Tittel (1994)."Video Reflectometry to Specify Optical Properties of Tissue *in vivo," Medical Optical Tomography*, pp. 211-226.

Johnson, C. C. (1970). "Optical difusion in blood," *IEEE Trans. Biomed. Engr.*, Vol. BME-17, pp. 129-133.

Judy, M. M., L. Fuh, J.L. Matthews, D.E. Lewis, R.E. Utecht (1994). "Gel electrophoretic studies of photochemical crosslinking of type I collagen with brominated 1,8-naphthalimide dyes," *Proc. Soc. Photo-opt. Instr. Eng., Laser Welding: Modeling, Delivery Systems, and Tissue Solders,* Vol. 2128E, in press.

Kanda, M., K. Awazu, M. Masuzawa, et al.(1988)."Continuous monitoring of cardiogreen removal by a diseased hepatic using an optical sensor," *SPIE*, Vol. 904, pp. 39-46.

Kellerman, A.L., C.A. Cofer and S. Joseph (1991)."Inpact of portable pulse oximetry on arterial blood gas test ordering in an urban emergency department," *Annals. of Emergency Medicine,* Vol. 20, pp. 130-134.

Kienle, A., R. Hibst, R. W. Steiner (1994)."Use of a neural network and Monte Carlo simulations to determine the optical coefficients with spatially resolved transmittance measurements," *SPIE*, Vol. 2134A, in press.

Landsman, M.L.J. and G.Kwant (1978)."Lightabsorbing Properties, stability, and spectral stabilization of indocyanine green," *J.Appl.Physiol.,* Vol.40, No.4, pp. 575-583.

Leevy, C., C. Mendenhall, W. Lesco and M. Howard (1962). "Estimation of hepatic blood flow with indocyanine green," *J. Clin. Invest.,* Vol. 41, pp. 1169.

Liu, H., M. Miwa, B. Beauvoit, N. G. Wang, B. Chance (1993). "Characterization of absorption and scattering properties of small-volume biological samples using time-resolved spectroscopy," *Anal. Biochem.*, Vol. 213, pp. 378-385.

Loh C.S., J. Bedwell, et al.(1992)."Photodynamic therapy of the normal rat stomach: a comparative study between di-sulphonated aluminum phthalocyanine and 5-aminolaevulinic acid," *Br. J. Cancer* Vol. 66, pp.452-462.

Malik Z., H. Lugaci (1987)."Destruction of erthroleukaemic cells by photoactivation of endogenous porphyrins," *Br. J. Cancer* Vol. 54, pp. 589-595.

McMahon, D.H. and A.R. Nelson (1981)."Fiber-optic transducers," *IEEE Spectrum,* Dec.-1981, pp. 24-29.

Mollenauer, L.F., R.H. Stolen and J.P.Gordon (1980)."Experimental observation of picosecond pulse narrowing and solitons in optical fibers," *Phys. Rev. Lett.*, Vol. 45, pp. 1095-1098.

Namihisa, T.(1969)."Report of Hepatic Function Study Japanese Society of Gastroenterology: Standard Operation Method of Indocyanine Green (ICG) Test," *Jpn J. Gastroenterol.* Vol.70, pp.573-574

Namihisa, T., K. Nanbu, K. Iijima et al.(1963)."Method of Liver function Test by Indocyanine Green," *Acta Hepatologica Japonica* Vol. 5, pp.114-120.

Namihisa, T., K. Awazu etal. (1990)."Multicenter study of indocyanine green tests by non-invasive optical finger piece method," *Kan.Tan. Sui* , Vol. 20, pp. 347-351.

Ohgoshi, T. (1983). *Optical fiber*, Ohm Publishing Inc., Tokyo.

Patterson, M. S. , B. Chance, B. C. Wilson (1989)."Time resolved reflectance and transmittance for the non-invasive measurement of tissue optical properties," *Applied Optics*, Vol. 28, pp. 2331-2336.

Patterson M.S., B.C. Wilson, R. Graff (1990)."In vivo tests of the concept of photodynamic threshold dose in normal rat liver photosensitized by aluminum chlorosulphonated phthalocyanine," *Photochem. Photobiol.* Vol. 51, pp. 343-349.

Patterson, M. S., J. D. Moulton, B. C. Wilson, K. W. Berndt, J. R. Lakowicz (1991)."Frequency domain reflectance for the determination of the scattering and absorption properties of tissue," *Applied Optics*, Vol. 30, pp. 4474-4476.

Paumgartner, G. and C. M. Leevy (1970)."Kinetics of indocyanine green removal from the blood," *Ann. N.Y. Acad. Sci.,*Vol. 170, pp.134-147.

Pickering, J. W. , S. A. Prahl, N. Vanwieringen, J. F. Beek, H. J. C. M. Sterenborg, and M. J. C. Vangemert (1993)."Double-integrating-sphere system for measuring the optical-properties of tissue," *Applied Optics*, Vol. 32, pp.399-410.

Plass, G. N., G. W. Kattawar and F. E. Catchings (1973). "Matrix operator theory of radiative transfer. 1: Rayleigh scattering," *Appl. Opt.,* Vol. 12, pp. 314-329.

Pologe, J. A. (1987)."Pulse oximetry; technical aspects of machine design," *Int. Anethesiology Clin.*, Vol. 25, pp. 137-153.

Potter W.R.(1989)."PDT dosimetry and response,"*SPIE* Vol. 1065, pp. 88-99.

Prahl, S. A. (1988). "Light transport in tissue," PhD. dissertation, the University of Texas at Austin, TX.

Prahl, S. A., M. Keijzer, S. L. Jacques and A. J. Welch (1989). "A Monte Carlo model of light propagation in tissue," *Proc. SPIE IS*, Vol. 5, pp. 102-114.

Reynolds, L.O. (1975). "Optical diffuse reflectance and transmittance from an anisotropically scattering finite blood medium," PhD. Dissertation, University of Washington, Seattle, WA.

Siegman, A.E. (1986). *LASERS:An introduction to lasers*, University Science Books, California, pp. 2-80.

Star, W. M. (1989). "Comparing the P3-approximation with diffusion theory and with Monte Carlo calculations of light propagation in a slab geometry," *SPIE IS* Vol.5, pp.16-22.

Steinmetz, L. (1983)."Characteristics of the linear array total internal reflection (TIR) electrooptic spatial light modulator for optical information," *Optical Eng.*, Vol. 22, pp. 665-675.

Stuart Ira Fox (1984). *Human Physiology*, Wm. C. Brown Publishers. pp.366.

Szaflarski, N. L. and N.H. Cohen (1989)."Use of pulse oximetry in critically ill adults," *Heart and Lung*, Vol. 20, pp. 444-455.

Szmant, H.(1971). "Chemistry of DMSO. In *Dimethyl sulphoxide 1*,"ed. Stanley W. Jacob, et al., Marcel Dekker, Inc., NY.

Takaki, N.K. and C.W. Mathews (1967)."Indocyanine Green Liver Function Studies on Women Taking Progestins,"*J.Obstet.Gynec*, Vol. 30, No.2, pp220-227

Takatani, S. (1980). "Noninvasive tissue reflectance oximeter: An instrument for tissue hemoglobin oxygen saturation i vivo," *Annals of Biomed. Engr.* Vol. 8, pp. 1-15.

Thomsen, S. L. , H. Vijverberg, S. L. Jacques, A. A. Oraevsky (1994). "Optical properties of albinao rat skin heated in vitro: comparison of photoacoustic and integrating sphere measurement techniques," *SPIE*, Vol. 2134A, in press.

Tomasovic S. P. (1983)."Hetero-geneous response and clonal drift of sensitivities of metastatic 13672NF mammary adenocarcinoma clones to g-radiation in vitro," *Cancer Res.*Vol. 43, pp.6-10.

Tromberg, B. J., L. O. Svaasand, T. T. Tsay, R. C. Haskell (1993). "Properties of photon density waves in multiple-scattering media," *Applied Optics*, Vol. .32, pp. 607-616.

Verdeyen, J.T. (1989). *Laser Electronics: Advanced topics in electromagnetics of lasers*, Prentice-Hall, Inc., New Jersey, pp. 453-510.

Wang, L.-H. and S. L. Jacques (1992)."Monte Carlo modeling of light transport in multi-layered tissues in standard C," The University of Texas M. D. Anderson Cancer Center, Houston, Texas, .

Wilson, B. C. and W. P. Jeeves (1987). "Photodynamic therapy of cancer," in *Photomedicine* Vol. II, Edited by E. Ben-Hur and I. Rosenthal, CRC Press, Boca Raton, Florida, pp. 127-177.

Wilson, B. C., and G. Adam (1983). "A Monte Carlo model for the absorption and flux distribution of light in tissue," *Med. Phys.* Vol. 10, pp. 824-830.

Wilson, B. C., T. J. Farrell, and M. S. Patterson (1990). "An optical fiber-based diffuse reflectance spectrometer for non-invasive investigation of photodynamic sensitizers in vivo," *SPIE,* Vol. 6, pp. 219-232 .

Yelderman, M. and W. New (1983)."Evaluation of pulse oximetry," *Anethesiology*, Vol. 59, pp. 349-352.

Yoshizawa, T. (1985). *A mannual for applied measurements in optics*, New Technology Development Center, Tokyo.

Yokosuka, H. , K. Nagayama, M. Horiguchi et al.(1986)."Improved ICG Earpiece and Its Application," *Basic Pharmacol. & Ther.* Vol. 14, Suppl. 2, pp. 223-232.

ACKNOWLEDGMENTS

Like any other research project this thesis required the efforts of many dedicated, enthusiastic, and supportive people. This page is where I have the opportunity to thank these people for their efforts. First, I wish to thank Professor Susumu Fujii, Kobe University, for providing support throughout this project. I also thank Professor Kenzo Akazawa, Kobe University, for encouragement and technical discussion. I express my deep thanks to Professor Yukio Tada, Kobe University, for reviewing this thesis.

The author thanks professor Nobuhiro Sato, and professor emeritus Toshihiko Namihisa of Juntendo University. The author also give grateful thanks to Dr. Hironaga Matsubara, Shin-ichiro Niwa, Masahiko Osawa, Yuichi Miyagawa and Junichi Kurihara, who are colleagues at Sumitomo Electric, for their contribution to the development. Moreover, we would like to thank members of Dai-ichi pharmaceutical company for their effort to clinical evaluation. I need to express my gratitude to Dr. Takio Tomimasu for his consideration of writing this thesis.

In additon, the authors thank Dr. Steven L. Jacques, Laser Biology Laboratory at The University of Texas, M.D. Anderson Cancer Center. I have learned an immense amount about the scientific process during the past two years from him. I am looking forward to continuing this learning experience both through my own research and by watching the progress of work at The University of Texas

MD Anderson Cancer Center and Sumitomo Electric. Steven L. Jacques has provided a much needed view - he helped to clearly define the problems, to limit the scope of the work to a manageable mass, and to encourage me to finish when the enormity of the writing seemed overwhelming. Jon Shwartz took on the job of my day-to-day advisor, a job I don't believe anyone ever officially asked him to assume. Tom is a renown biologist who instructed me in a number of areas that I now realize take a lifetime, or more, to master: experimental design. A number of other specialists have contributed to this work: Shousuke Yamanouchi has provided general guidance; Lihong Wang has always been available to discuss light propagation and ablation mechanisms; Sharon Thomsen brought clinical perspective and unabashed curiosity to the research when it was needed; Dr. Ichiro Nishizaki, my friend, has encouraged me to tackle this thesis.

Finally, I close with deep thanks to my family. My parents, Shigekazu and Sae have encouraged and supported my education every step of the way. My mother-and father-in-law have helped in innumerable ways. My daughter, Yukiko, has endured my absence on and off over the last year as I finished my research and tackled the task of writing this thesis; I was also unable to spend as much time with my son, Toshikuni, as I would have liked. I am now greatly looking forward to watching and '~guiding~ these two energetic and inquisitive people as they grow. Lastly, but most importantly, Keiko. She has had the hardest job of all - while raising two kids and

helping her never-present husband further his career. Given the turmoil of life this past year, she's done a truly remarkable job.